Transformation between the Johnson-Cousins and Sloan Photometric Systems for SSA

Philip J. Castro [1], Tamara E. Payne[1], Joseph W. Moody [2], Stephen A. Gregory[1], Phan D. Dao[3], Roberto I. Acosta[4]

[1]Applied Optimization
3040 Presidential Drive, Suite 100
Fairborn, OH 45324

[2]Brigham Young University
Department of Physics and Astronomy
Provo, UT 84602

[3]Air Force Research Laboratory
Space Vehicles Directorate
Kirtland AFB, NM 87117-5776

[4]NASIC/GSMS
4180 Watson Way
WPAFB, OH 45433-5648

Abstract

Space Situational Awareness (SSA) observations are sometimes performed through a spectral filter. The traditional filters used are those of the Johnson-Cousins photometric system (*B*, *V*, *R*, and *I*). The SSA community has been observing with these filters for decades and therefore has historical data spanning this duration. More recently, the astronomical community is replacing the Johnson-Cousins system with the Sloan photometric system as the primary system for optical observations. The most recent large astronomical surveys in the optical regime have used the Sloan filters: the Sloan Digital Sky Survey and the Panoramic Survey Telescope and Rapid Response System (Pan-STARRS). The Pan-STARRS 1 catalog sky coverage and its astrometric and photometric precision make it well suited for in-frame calibrations of satellite observations. Such in-frame calibrations would provide increased calibration cadence and the potential for improving accuracy by mitigating the effects of a changing atmosphere. Because a comparable catalog in the Johnson-Cousins photometric system that would allow in-frame calibrations does not exist, it makes sense for SSA observations to transition to the Sloan system. A consequence of transitioning from Johnson-

Cousins to Sloan is the obsolescence of the historical Johnson-Cousins satellite photometry. To compare photometry between the Johnson-Cousins and Sloan systems, a transformation needs to be made to convert data from one photometric system to another.

A number of such transformations exist within the astronomical community for stellar objects. However, the Spectral Energy Distributions (SEDs) of stars are not the same as those of satellites. Reflection for spacecraft can be modeled based on diffuse and specular reflection components, where the diffuse components' reflected spectrum may have spectral characteristics of the material off which it reflects, thereby altering the SED from that of the Sun. While the SEDs of stars are largely static, the SEDs of satellites are not. Specifically, their SED may change with phase angle (e.g., solar panel contributions are phase angle dependent and typically make the SED bluer). To investigate the transformation between Johnson-Cousins and Sloan for satellites, we performed the following analysis. We observed four satellites sequentially in Johnson-Cousins filters (*B, V, R,* and *I*) and Sloan filters (*g′, r′, i′,* and *z′*), covering a large range of phase angle. We then empirically derived transformations between Johnson-Cousins and Sloan for each satellite's observed data and for all of the observed satellite data as a whole, and juxtaposed these with an astronomical transformation. We found mixed results for the transformation relations. The $r' - V$ as a function of $V - R$ relation provides a great fit for all of the observed satellite data with low root mean square (RMS) error and is exactly the same as the astronomical transformation. The $r' - z'$ as a function of $R - I$ relation provides a great fit for all of the observed satellite data, but has large RMS scatter and is distinct from the astronomical transformation. Thus, we do not recommend transforming historical satellite photometry observed in Johnson-Cousins to Sloan to compare to observations of satellites taken in the Sloan filters. Since the transformations are dependent on the SED of the satellite, and the satellites' SEDs are variable, transformations generally yielded poor results for the two photometric systems we studied here, i.e. Johnson-Cousins and Sloan. Moreover, our supposition is that such attempts with any two photometric systems may yield similarly poor results.

1. INTRODUCTION

The Johnson photometric system is based on a set of filters and detectors in the optical wavelength region; the *UBV* spectral regions were established by [1], and [2] later added the *RI* spectral regions [3]. An additional *RI* system was also defined by [4], and Cousins [5] later modified this *RI* system [6]. The final definition of the Johnson-Cousins standard system ($UBVR_CI_C$) is the result of extensive work by Arlo Landolt [7]. He published a list of standard stars in the *UBV* system and [6] extended this list to include stars in the Cousins *R* and *I* bands. Most astronomers use Landolt standard stars to transform their system to that of the Johnson-Cousins system [8]. The Johnson photometric system has been used by the astronomical community for decades [7] [6] [9] [10] [11]. For a more thorough discussion of the development and evolution of the Johnson system, see [6] and [3]. This photometric system has historically been used for filter observations of satellites [12] [13].

The original Johnson-Cousins bandpass profiles were determined by the technology of their time. Although a very useful system, the filter bandpasses tend to be round with large, overlapping wings (see Fig. 4). Modern filters can be constructed with much sharper cut-on and cut-off slopes, making their measured wavelength range more precise. Because of this, the astronomical community is tending to replace the Johnson filters with the Sloan filters [14] as the primary photometric system for optical observations. The most recent large astronomical surveys in the optical regime use the Sloan filters, beginning with the Sloan Digital Sky Survey (SDSS) [15] [16] that introduced the Sloan photometric system [14], and most recently with the Panoramic Survey Telescope and Rapid Response System (Pan-STARRS) [17] [18].

Both of these surveys use what is generally referred to as the Sloan photometric system, although individual differences exist between the filters used by SDSS and those used by Pan-STARRS [17]. The SDSS was designed to survey the northern galactic cap and parts of the southern cap and therefore does not have complete coverage of the celestial equator and the northern hemisphere [16]. The shallower but more expansive Pan-STARRS 1 (PS1) project has surveyed the 3π steradians north of -30 degrees declination. A major goal of the survey was to construct a precision

photometry reference catalog covering the entire 3π region [18]. The PS1 filters are g_{P1}, r_{P1}, i_{P1}, z_{P1}, y_{P1}, with the subscript to distinguish the PS1 photometric system from others.

The coverage and precision photometry of Pan-STARRS make it well suited to serve as a catalog for in-frame calibrations for satellite observations. In-frame calibrators would allow more accurate calibrations for atmospheric conditions that may change throughout the night and therefore are preferable when compared to all-sky calibrations. In-frame calibrations in the Johnson-Cousins system are not feasible due to the absence of a catalog that covers a large enough region of the sky; standard stars by [10] were scattered mostly near the equatorial region. By transitioning observations of resident space objects from the Johnson-Cousins system to Sloan, in-frame calibrations are attainable.

A consequence of transitioning from the Johnson-Cousins system to the Sloan system is that the catalogs of GEO satellite photometry using the Johnson-Cousins photometric system may become obsolete. In order for the historical data to not become obsolete, it is important to transform the satellite photometry from Johnson-Cousins to Sloan.

The Sloan Digital Sky Survey (SDSS) photometric system, or the Sloan photometric system, was introduced by [19]. This system is composed of five bands ($u'g'r'i'z'$) that begin at the ultraviolet cutoff of 3000 Angstroms to the sensitivity limit of a silicon CCD at 11,000 Angstroms (see Fig. 4). The Sloan photometric system is on the AB magnitude system, which allows an immediate conversion from magnitudes to physical fluxes while the Johnson-Cousins system is on the Vega magnitude system [3]. The Sloan pass bands are wider and essentially non-overlapping while the Johnson-Cousins filters overlap considerably [20]. Reference [19] calculated linear transformation equations from the Johnson-Cousins system to the Sloan system using synthetic magnitudes from the spectrophotometric atlases of [21] and [22]. These transformations were a function of one Johnson-Cousins color. The $r' - i'$ transformation was broken up into two linear transformations at $R_c - I_c = 1.15$, and the $r' - z'$ transformation was also broken up into two linear transformations at $R_c - I_c = 1.65$.

Reference [20] published a list of standard stars that defined the $u'g'r'i'z'$ photometric system and provided the basis for the photometric calibration of SDSS. They also calculated linear transformations between Johnson-Cousins and Sloan systems using observed data, in contrast with [19] who used synthetic photometry. These transformations are a function of one Johnson-Cousins color. They break up the $r' - i'$ as a function of $R - I$ transformation into two linear transformations, one with $R - I < 1.15$ mag and one with $R - I \geq 1.15$ mag.

Reference [23] performed a comparison between the Palomar-Green (PG) Bright Quasar Survey (BQS) and SDSS to investigate the extent to which the survey is complete and representative of the general quasar population. Since the Palomar-Green observations are in Johnson *U* and *B* filters, it was necessary to derive transformations between Johnson-Cousins and Sloan. However, the set of filters provided to the U.S Naval Observatory (USNO) 1m telescope used to establish a standard star network were not stored in a vacuum while those of the SDSS were. As a consequence the layers in the interference filter coatings of SDSS shrank slightly, shifting the red edge blueward and changing their photometric values slightly. Therefore the standard stars of the USNO 1m telescope define the $u'g'r'i'z'$ photometric system as discussed in [20], while the data from the SDSS 2.5 m telescope [24]was in the *ugriz* system. This means the system that established the standard star network ($u'g'r'i'z'$) is not the same as that of SDSS (*ugriz*); these are small but important differences. These systems were predicted to differ systematically at a few percent for $g'r'i'$ and slightly more for the u' and z' [3] [20] [23].

Transformations exist between these two systems ($u'g'r'i'z'$ and *ugriz*) [23]. Reference [23] transformed the standard stars on the $u'g'r'i'z'$ system to the *ugriz* system. They used only those standard stars with $U - B < 0$ and $R - I < 1.15$, and calculated linear transformations between Johnson-Cousins and Sloan. They used a subset of the standard stars of the Sloan photometric system [20] that also have measurements in the Johnson-Cousins photometric system from Arlo Landolt [9]. A transformation was also determined for all SDSS standard stars regardless of a $U - B$ cutoff and $R - I < 1.15$. Reference [23] notes that stars with $R - I < 1.15$ have a different color transformation than stars with $R - I \geq 1.15$, but there is not a sufficient number of stars with $R - I \geq 1.15$ to derive a transformation. Reference [23] suggests that separate transformations should be derived for stars of different spectral classes because of differences in the

strength of the Balmer lines, especially between white dwarfs and the remaining blue stars. Synthetic photometry suggests that some white dwarfs (those of spectral class A and luminosity class D) have a $B - g$ that is greater by approximately 0.1 mag than that of the remaining white dwarfs and hot subdwarfs. However, there are not enough stars with accurate spectral classifications and Johnson-Cousins photometry to determine this using observed data. Reference [23] developed separate transformation equations for quasars: "To account for the different spectral shapes of stars and quasars, in particular the presence of strong emission lines, we derive separate transformation equations for quasars." [23]. Transformations for quasars are determined via synthetic photometry of composite quasar spectra in the SDSS and Johnson-Cousins systems. All of their transformations (stars and quasars) are a function of one Johnson-Cousins color.

Reference [25] determined linear transformations between Johnson-Cousins and Sloan using 224 stars with *UBV* data from [9] and observed with the CASU INT Wide Field Survey in $u'g'r'$. Their data collected by the CASU INT Wide Field Survey is based on the throughput of their system, so there will be differences between their photometry and that of SDSS. They determined transformations for $g' - r'$ and $u' - g'$. Unlike previous work, their transformations for the Sloan colors, $g' - r'$ and $u' - g'$, are a function of two Johnson-Cousins colors, $U - B$ and $B - V$.

Reference [26] derived transformations using SDSS DR4 (*ugriz*), and Johnson-Cousins photometry from Stetson [27] that was published in January 2005 and Landolt stars [9]. Only SDSS photometry from the catalog we created for [[28] was used. The Landolt stars contain mostly Population I stars, while Stetson's newer fields also include Population II (metal-poor) stars. They derive transformations that are linear using all of their data, without distinction between Population I and Population II stars. These transformations are a function of one Johnson-Cousins color, except for the $u - g$ transformation being a function of two colors, $U - B$ and $B - V$, as was done in [25]. The $r - R$ was broken up into two distinct linear transformations at $V - R = 0.93$. To assess the effect of metallicity on the transformations, they also derive transformations for Population I and metal-poor Population II stars. Stars were selected from Stetson to compose the metal-poor Population II stars, while the Landolt stars metallicity is unknown. However, it is assumed that most of them belong to the Galactic disk which is composed of mostly Population I stars that have a range of metallicity, and are more metal-rich than the Population II sample. These transformations are linear and are a function of one Johnson-Cousins color. The $r - R$ transformation for Population I stars is broken up at $V - R = 0.93$, while the $r - R$ transformation for metal-poor Population II stars is only valid for $V - R \leq 0.93$ due to an absence of metal-poor Population II stars with $V - R > 0.93$. The Population I and metal-poor Population II transformations result in slightly different slopes. Significant scatter is present in the $V - R$ vs. $r - R$ and $R - I$ vs. $i - I$ color-color diagrams for the metal-poor Population II stars, with the data from these diagrams indicating a poor relation to the linear fit.

Reference [29] determined transformations for main sequence stars (luminosity class V) that are common between the Johnson-Cousins $UBVR_CI_C$ photometry from [9] and the Sloan $u'g'r'i'z'$ photometry from [20]. They demonstrate that there is a dependence of the transformation on luminosity class, and, for this reason, unlike transformations discussed by other authors, only derive a transformation for main sequence stars. They point out that their transformations give better results than those of [25] and [20]. The typical RMS scatter of the transformations is of the order of 0.001 mag. Unlike the single color Johnson-Cousins dependence on the transformations, except for [25] and [26], the transformation of [29] determined the functional dependence based on the spectral overlap of the Johnson-Cousins and Sloan filters. They determined that the u' filter overlaps the U filter, the g' filter overlaps the B and V filters, and that therefore the $u' - g'$ color should be a function of $U - B$ and $B - V$. The V filter overlaps the g' and r' filters; therefore the $g' - r'$ color should be a function of $B - V$ and $V - R_C$. The i' and z' filters are not as clear and are a function of the detector being used due to the quantum efficiency cutoff at longer wavelengths. This resulted in some transformations that are a function of two Johnson-Cousins colors. They determined transformations for $u' - g'$ as a function of $U - B$ and $B - V$, $g' - r'$ as a function of $B - V$ and $V - R_C$ and was constrained to $V - R_C < 0.8$ mag, $r' - i'$ as a function of $R_C - I_C$, $r' - z'$ as a function of $R_C - I_C$, and $g' - V$ as a function of $B - V$. The $g' - V$ transformation is a quadratic expression (non-linear), while all of the other transformations are linear. They suggested additional work

to fully develop a complete set of transformations for all luminosity classes and to investigate the effects of metallicity on the transformations.

Reference [30] calculated transformations for a sample of cool stars using observations from the University of Washington 30-inch telescope at Manastash Ridge Observatory with the *V*, *R*, *I* Johnson-Cousins filters and the *r*, *i*, *z* Sloan filters. Previous studies, [20], [26], and [29], have examined $r - i$ less than or slightly beyond 1.5 mag (approximately a spectral type of M4), the work of [30] samples a redder population ($r - i > 1.4$, later spectral type). They derive transformations for $R - I$ as a function of $r - i$, $V - R$ as a function of $r - i$, $R - I$ as a function of $i - z$, and $r - i$ as a function of $V - I$; the transformations are a function of a single color. All of these transformations are polynomials to the power of three; they are not linear. They find that the $R - I$ vs $r - i$ color transformation, when compared to [26] and [29], agrees within the uncertainties.

Fig. 1 shows the astronomical transformations for Johnson-Cousins and Sloan ($g' - V$ vs. $B - V$) from the literature discussed above. Transformations for both *g* (unprimed) and *g′* (primed) are included and indicated in the legend. The range of data shown is based on a common *B*–*V* overlap ($B - V$ = -0.2 to 1.7 mag) of the transformations from the different authors; $B - V$ ranges for [23] were not available. All of the transformations are for stars, except for the one transformation for quasars as indicated in the legend. Note the transformations of [23] and [26] are on the Sloan *ugriz* system and not the *u′g′r′i′z′* system. The transformation from [26] is for their entire sample: Population I and Population II stars. References [25] and [30] did not have $g' - V$ vs $B - V$ transformations and therefore are not included in the figure. All of the transformations for the stars are comparable, with a spread of approximately 0.075 mag at the blue end ($B - V$ = -0.2 mag) and 0.15 mag at the red end ($B - V$ = 1.7 mag). Some of this spread is due to differences in the unprimed and primed Sloan transformations. The transformation for quasars is markedly different from that of stars, similar to unprimed stellar transformations at the blue end and deviating from the unprimed stellar transformations at the red end by approximately 0.25 mag. The primed Sloan transformations group together at the red end and also at the blue end, where they start to overlap with the unprimed Sloan transformations that are grouped together. At the red end, the unprimed Sloan transformations are not grouped together as tightly.

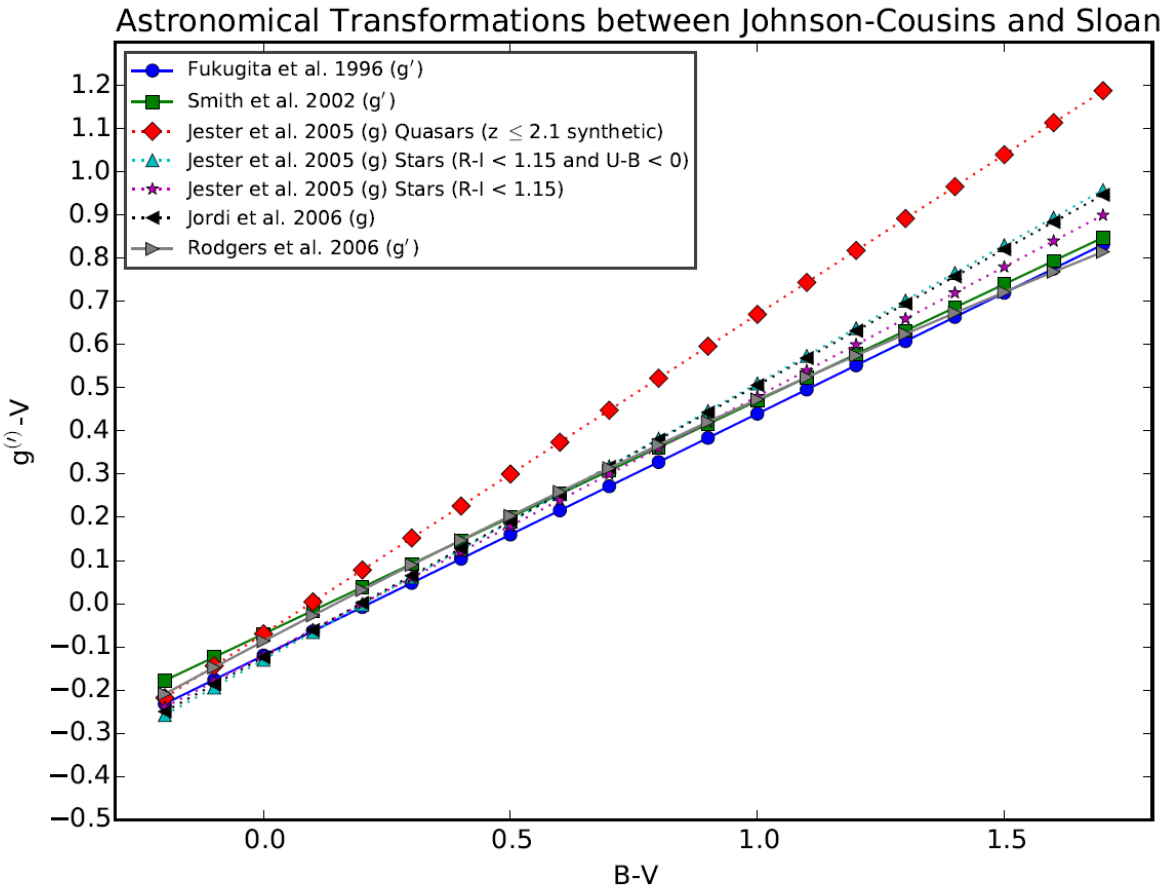

Fig. 1. Astronomical Transformations between Johnson-Cousins and Sloan from the literature.

The astronomical community developed transformations by sampling a population of stars; the largely static Spectral Energy Distribution (SED) of these stars served as the template with which to map the transformation. For satellites, instead of using a large population of satellites, we instead use the dynamic SED of a satellite or satellites as the template with which to map the transformation. The literature has shown that when the SED changes from that of a stellar SED, such as that of quasars, the transformation may not be the same. This warrants an investigation into the transformations for satellites to determine whether they are similar or dissimilar to that of the astronomical transformations. To empirically investigate a transformation between Johnson-Cousins and Sloan for satellites, we observed four satellites in BVR_CI_C and $g'r'i'z'$ asynchronously for one night.

We present our observations in Section 2, followed by our analysis of a transformation between Johnson-Cousins and Sloan for the collected satellite data in Section 3, and finally our conclusions in Section 4.

2. OBSERVATIONS

We use the data collected and reported on previously in [31]. That study investigated the discrimination ability for geosynchronous satellite data collected in the Johnson-Cousins and the Sloan photometric systems. For completeness we provide a description of the observing facility, targets, observations, and processing; most of this can also be found in [31].

2.1 ROVOR

ROVOR: The Remote Observatory for Variable Object Research ([32]; ROVOR) is located in central Utah at 39°27'17.1'' N, 112°43'01.0'' W and 1396 meters above sea level. The telescope is a 0.4 m RC Optical tube on a German-equatorial Paramount ME pier. The optics have an f/9 focal ratio in an open truss configuration with a primary mirror ion milled to 1/30 wave RMS. The sensor is an FLI ProLine PL003 with a back-illuminated 1024 × 1024 pixel SITe detector, with pixel size of 24 x 24 micron. The sensor has a readout time of about three seconds without binning. The filter wheel is a 12-position FLI Centerline equipped with a set of 50 mm square Astrodon Johnson-Cousins BVRI and Sloan $g'r'i'z'$ filters. The FOV is 23.4 x 23.4 arc-minutes with a plate scale of 1.37 arc-seconds per pixel. Pointing is accurate to better than 30 arc-seconds within 45 degrees of the zenith.

2.2 Targets

Four RSOs in geosynchronous orbit were observed. These were chosen for their observability from ROVOR and because they represent various satellite bus types. The description of these satellites is shown in Tab. 1. Given that there are a limited number of space-worthy satellite materials, it is assumed that this set of RSOs samples the material variations adequately enough that this sample size is not biased. Notional artist renderings of the satellites are shown in Fig. 2.[1]

Tab. 1. Description of Geosynchronous satellites observed for this research.

Satellite Descriptions				
Number	**Name**	**Launch Date**	**Bus Type**	**Country**
25740	NIMIQ-1	1999-05-20	Lockheed Martin A2100AX	Canada
38342	NIMIQ-6	2012-05-17	Loral Space Systems SSL-1300	Canada
37809	SES-2	2011-09-21	Orbital Star-2.4	USA
32018	SPACEWAY-3	2005-11-16	Boeing BSS-702	USA

Fig. 2. Notional artist renderings of the four satellites observed for this research.

[1] Internet source: Gunter's Space Page, http://space.skyrocket.de/

The RSOs were observed throughout the night in order to obtain as much phase angle diversity as possible. On the night of May 11-12, 2016 (i.e. May 12 UT), we successfully observed the satellites NIMIQ-1 (25740), NIMIQ-6 (38342), Spaceway-3 (32018), and SES-2 (37809) in the Johnson-Cousins filters *BVRI* and Sloan *g'r'i'z'* at each pointing. We observed standard stars SA107-351, SA107-1006, and SA109-381 for calibration purposes; these were interspersed throughout the night. The sequence and details of the observations is given in Tab. 2. We note that the observations were performed outside of glint season, and therefore our analysis will be representative of satellites during the non-glint season.

Tab. 2. Basic observational data

Object	**Exposure Times (sec)**								**Comments**
	B	*V*	*R*	*I*	*g'*	*r'*	*i'*	*z'*	
NIMIQ-1 (25740)	6	4	2	3	3	3	3	5	33 pointings 1 frame in each filter, starting at 4:45:20 UT
NIMIQ-6 (38342)	8	6	6	6	6	6	6	6	33 pointings 1 frame in each filter, starting at 4:48:51 UT
SPACEWAY-3 (32018)	6	4	3	3	3	3	3	5	33 pointings 1 frame in each filter, starting at 4:50:29 UT
SES-2 (37809)	6	4	3	3	3	3	3	5	33 pointings 1 frame in each filter, starting at 4:46:56 UT
SA107-351	60	30	30	30	30	30	30	30	3 pointings of 3 frames in each filter; Mid-point airmasses: 1.96, 1.54, 1.36
SA107-1006	60	30	20	20	30	20	20	30	3 pointings of 3 frames in each filter; Mid-point airmasses: 2.07, 1.59, 1.38
SA109-381	60	30	30	30	30	30	30	30	3 pointings of 3 frames in each filter; Mid-point airmasses: 1.58, 1.41, 1.32

The weather was photometric to the eye and the date of observation was in the middle of a four-day long clear pattern so we expected the results to be accurate and they were. The photometry was extracted from the calibrated image frames using aperture photometry methods. The instrumental magnitude was corrected for extinction via the formula below.

$$v_o = -2.5\log_{10}(\text{counts/sec in V}) + A_v X$$

where v_o is the instrumental magnitude, X is the airmass, and A_v is the extinction coefficient. The above formula is for V explicitly, but the same formula was applied to all the band passes. Extinction coefficients are given in Tab. 3. The error quoted is the standard error, which is the RMS of the values found for the three different stars divided by the square root of the number of stars sampled, which was three.

Tab. 3. Extinction Coefficients, A_x

Filter	Coefficients (magnitudes/airmass)							
	V	B	R	I	g'	r'	i'	z'
Extinction, *A*	0.270	0.155	0.108	0.074	0.231	0.115	0.094	0.088
Error	0.006	0.007	0.006	0.018	0.018	0.013	0.026	0.035

The values of the coefficients for the filter solutions are given in Tab. 4. The internal error is the RMS scatter in the value of (standard value – instrumental value) of each star added in quadrature. That is, it is formed with the value of (standard value – instrumental value) for all measurements in a particular filter for each standard star. Then the values are added together for the three stars using the relation:

$$Internal\ Error = \sqrt{\frac{RMS_1^2 + RMS_2^2 + RMS_3^2}{3}}$$

The total error is the deviation between the three stars. It is larger than the internal error because it also includes the uncertainty caused by applying no color correction. That is, the internal error is dominated by the Poisson statistical scatter in the data, while the total error is dominated by the differences in the colors of the standard stars. The tabulated coefficients in Tab. 3 and Tab. 4 were used to transform all satellite data into standard magnitudes.

Tab. 4. Standard calibration coefficients

Filter	Coefficients							
	B	V	R	I	g'	r'	i'	z'
Zero point ζ (magnitudes)	20.160	20.199	20.379	19.525	20.706	20.460	20.080	19.223
Internal error	0.0051	0.0072	0.0052	0.0058	0.0076	0.0070	0.0059	0.0099
Total error	0.015	0.009	0.010	0.040	0.045	0.035	0.060	0.091

An extinction plot for the standard star SA109-381 is shown in Fig. 3, this shows that the observing conditions throughout the night were stable and photometric. Similar plots for the other two standard stars show the same results. The symbols represent the data and the dotted lines show the linear fit through the data for all eight filters.

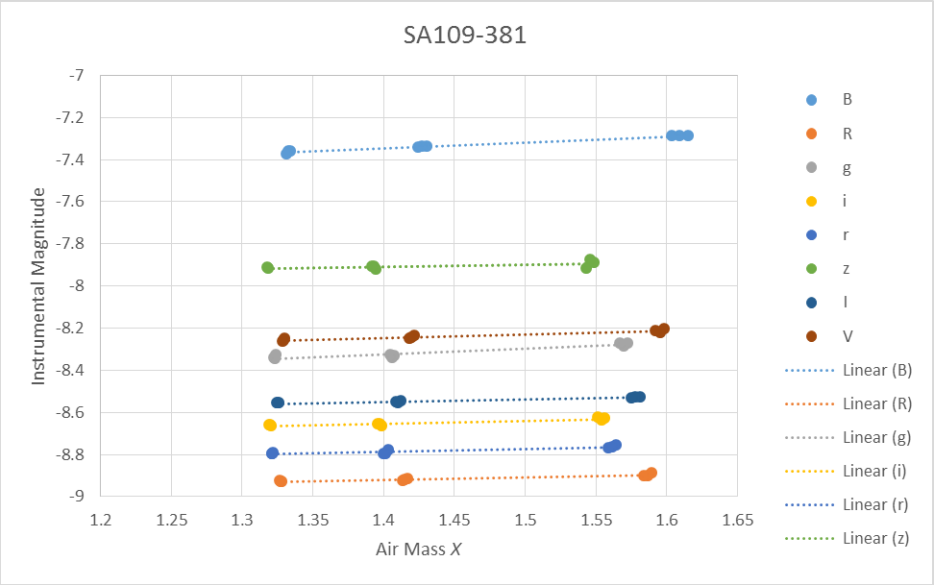

Fig. 3. Extinction plot, instrumental magnitude plotted against airmass for SA109-381.

3. ANALYSIS

Three themes are present throughout the literature for astronomical transformations between Johnson-Cousins and Sloan. We summarize them below.

1) When the SED of the underlying sample changes, then the transformation may not be the same. This was demonstrated by [23] where a different transformation was calculated for quasars because their SED is different than stellar SEDs. The transformation for quasars is clearly different than that of the stellar population. For [26], the slightly different transformations for Population I and metal-poor Population II stars may be due to their differing SEDs. In addition, the metal-poor Population II stars do not necessarily show a linear trend in some of the color-color diagrams, containing significant scatter about their linear fit and showing a poor relation to the linear fit. This theme is also present for [29] who show that the transformations are dependent on luminosity class. By developing a transformation for just main sequence stars (luminosity class V), a transformation is developed for a specific set of SEDs that shows an improved transformation over other work that has grouped stars with different SEDs together. We can apply this same principle to transformations between Johnson-Cousins and Sloan photometry for satellites. If the SED of satellites is different from that of stars then the transformation may also be different.

2) The transformations are sometimes linear and sometimes they are not. References [29] and [30] have at least one transformation that is non-linear, while the other references have linear transformations.

3) Lastly, the transformations from Johnson-Cousins to Sloan are a function of a single Johnson-Cousins color, and sometimes they are a function of two Johnson-Cousins colors. References [25], [26], and [29] have at least one transformation that is a function of two Johnson-Cousins colors, while the other references have transformations that are a function of one Johnson-Cousins color. These last two themes provide a range of options when determining a transformation between Johnson-Cousins and Sloan for satellites. The transformation is a function of the filter transmission curves of both photometric systems and the underlying SED of the sources.

Under specific conditions, the geometrical reflecting properties of a surface are characterized by the bidirectional reflectance distribution function (BRDF). Based on the BRDF of a material, the reflected intensity is a function of the incident and reflected angles and is also be a function of wavelength. The reflected intensity is a function of both diffuse and specular components, where the diffuse components reflect light equally in all directions and the specular

component reflects more light in some directions than others. In the latter case, there is a dependence on the location of the observer [33] [34].

Reflection for spacecraft can be modeled based on two components of reflection, diffuse and specular, with the Sun as the illumination source. The diffuse component scatters light equally in all directions and has a reflected spectrum that may include spectral characteristics of the material off which it reflects, while the specular component reflects light in a mirror-like manner and is assumed to be similar to the Sun's spectrum [34] [35]. "In general, the surface of a satellite will selectively reflect or absorb certain wavelengths giving rise to a reflectance spectrum that is uniquely characteristic of the chemical composition of the surface." [36]. Primarily diffuse reflected light dominates most of the phase angle signatures for a majority of geosynchronous photometric monitoring. At times of specific alignment between the satellite, observer, and Sun, specular reflection of relatively flat surfaces such as solar panels can cause a brief and very large increase in reflected light dominating the diffuse signature, referred to as a glint [37]. Solar panels are designed to absorb most of the visual spectrum, with preference toward the redder part of the spectrum containing most of the solar energy flux. Therefore, during such a solar panel glint, more blue light of the solar SED is reflected [35].

The SED of a satellite is a function of 1) the material properties of the satellite, 2) the illumination conditions, 3) the observer location, 4) the season, and 5) the attitude of the satellite. We consider each of these below.

1) The SED of a satellite is based on the Sun (G2V spectral type) reflecting off of materials on the surface, which may cause the SED to change from that of a G2V to a SED that is different than that of the Sun, depending on the reflectance properties of the material (BRDF) and the conditions under which the material is being viewed.

2) The SED is a function of illumination conditions as viewed by an observer. The Sun-satellite-observer angle (e.g., phase angle) [38] determines how much of the satellite is illuminated from the perspective of an observer. The SED may change based on the region of the satellite being illuminated if the material properties are different for diverse illumination conditions (phase angles). For example, if the materials on the East side of the geosynchronous satellite are a different color than the materials on the West side, then the SED will change as different portions of the satellite are illuminated. The SED can also vary on short timescales throughout the night.

3) There are two considerations here: a) The SED is a function of the location of the observer. Based on the BRDF of a material, the reflected intensity is a function of the reflected angle and therefore would depend on the observer location, since a larger or smaller contribution from the specular component in the reflected light would alter the SED. b) Viewing angle plays a role. If the same satellite were observed by an observer in the northern, eastern, southern, and western United States, for example, under the same illumination conditions (phase angle), the portions of the satellite that can be observed by one observer compared to the other varies slightly. If the material properties as viewed from the different observers varies, then the SED will also be different.

4) The SED is a function of season due to the Sun illuminating the satellite more northerly or southerly based on the time of year. If the illuminated material properties are different along the northern/southern direction, then the SED will change with season. In addition, the incident and reflected angles on the satellite facets will also change seasonally, which alters the SED due to varying degrees of a specular component in the reflected light.

5) If the attitude of the satellite changes, then the angle between the Sun, satellite facet, and observer has changed. The incidence and reflected angles of the material has changed and may alter the type of reflected light, diffuse or specular, depending on the BRDF of the materials being illuminated. This would alter the SED of the reflected light. Based on all the ways the SED of a satellite can change, it is clear the SED of a satellite is dynamic in time and dependent on the position of the observer.

A given observation of a satellite will in general be composed of the illuminated components of the satellite that are a superposition of diffuse and specular reflectances. The color index of a satellite is the ratio of fluxes of two spectral bands and is therefore a representation of the general shape of the SED covered by the two bands. The general results of our observations are presented in [31], and will not be repeated here. Their figures 10 - 13 show the color index

signatures of the four geosynchronous satellites for $B - R$, $V - I$, $g' - i'$, and $r' - z'$, respectively. These color indices are not static throughout the night in $B - R$, $V - I$, $g' - i'$, and $r' - z'$. The color index of the Sun is $B - R = 1.19$ mag and $V - I = 0.88$ mag, page 341 [39]. The B-R color index deviates moderately from the solar index for two of the satellites and deviates strongly for the other two satellites, with a maximum deviation from solar on average of 0.4 mag for one of the satellites. The $V - I$ color index for all of the satellites deviates from solar with a maximum deviation from solar on average of 0.45 mag for one of the satellites. It is also shown that these satellites can have different color index values from each other.. This demonstrates that the SED of each satellite is different. It is an ill-conceived assumption that it is valid to transform the Johnson-Cousins/Sloan photometry of a satellite from one system to another by using the astronomical transformations that were created from stellar SEDs.

For our observed satellite data we investigate all six of the astronomical transformations of [20], $g' - V$ as a function of $B - V$ relation, $r' - V$ as a function of $B - V$ relation, $r' - V$ as a function of $V - R$ relation, $g' - r'$ as a function of $B - V$ relation, $r' - i'$ as a function of $R - I$ relation, and $r' - z'$ as a function of $R - I$ relation. These are linear transformations based on observations that are a function of one Johnson-Cousins color, and are in the Sloan primed system, as are our Sloan observations. For the $r' - i'$ as a function of $R - I$ transformation, we use the $R - I < 1.15$ mag expression since we have no observed satellite data with $R - I \geq 1.15$ mag. By comparing our satellite transformations to the astronomical transformations of [20] we enable a uniform analysis since these astronomical transformations are linear and a function of one Johnson-Cousins color, unlike those of [29]. The astronomical transformations of [29] differ for two of the relations listed above. The $g' - V$ relation is a function of $B - V$ but is quadratic, and the $g' - r'$ relation is a function of $B - V$ and $V - R$.

Fig. 4 shows the Astrodon[2] transmission curves for the Johnson-Cousins ($UBVR_CI_C$) and the Sloan ($u'g'r'i'z'$) photometric systems used for our observations. Based on a visual inspection of the overlap of the filters between the two photometric systems, the functional relationship for transformations can be estimated. The g' filter is overlapped by the B and V filter. The r' filter is overlapped by the V and R filter, where it is completely overlapped by the R filter but not the V filter. The i' filter is overlapped by the R and I filter but not completely overlapped by either. Lastly, the z' filter is overlapped slightly by the R filter and the I filter. Therefore, the g' relation should be a function of B and V, the r' relation a function of V and R, and the resulting color index, $g' - r'$, a function of B, V, and R. The $r' - i'$ color index is a function of R and I. Finally, the $r' - z'$ color index is also a function of R and I. Note that we are comparing the satellite transformations to the relations of [20] who have the $g' - r'$ relation as only a function of $B - V$ and not as a function of B, V, and R as described for our filters.

Our transformations are also like the relation of [29] who use the $g' - r'$ relation as a function of $B - V$ and $V - R$. The R filter is desired in our case because the V filter does not completely overlap the r' filter. Therefore, the results for this relation will need to be interpreted with this in mind.

[2] From https://farpointastro.com/product-category/shop-by-brand/astrodon/

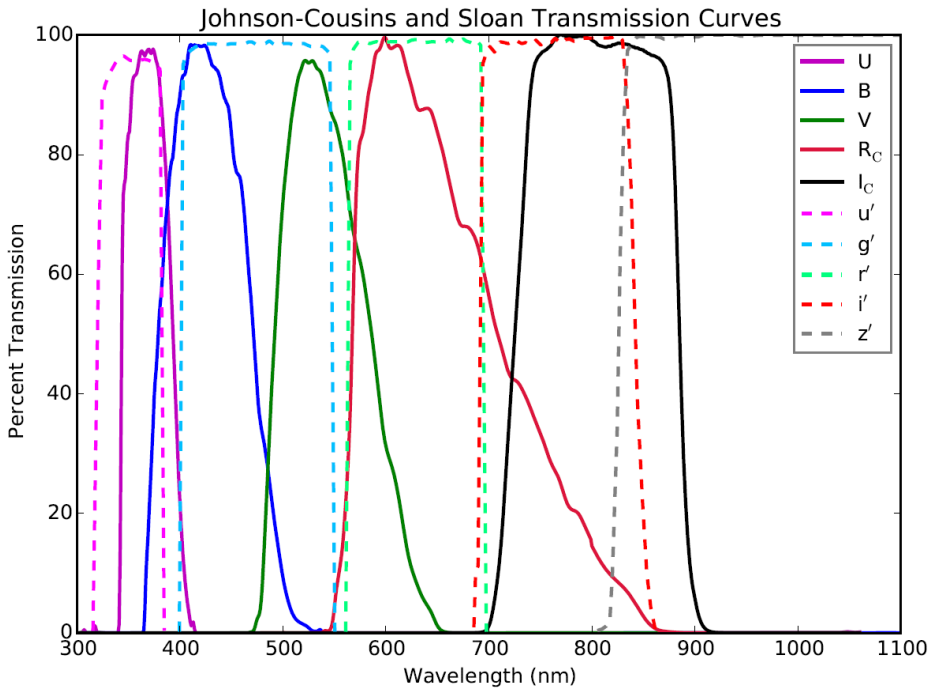

Fig. 4. Astrodon transmission curves for the Johnson-Cousins ($UBVR_CI_C$) and the Sloan ($u'g'r'i'z'$) photometric systems.

We perform an analysis of each satellite by determining a transformation based on the observed data and compare the satellite's transformation to that of the astronomical transformation of [20]. We then perform an analysis using all the satellite data together and determine a total satellite transformation. This is also then compared to the astronomical transformation. For each transformation we calculate the difference between the observed data and the satellite transformation, and the observed data and the astronomical transformation in order to provide an estimate of what errors may occur if using our derived satellite transformation or the astronomical transformation, respectively. We present our results for each of the relations in turn, beginning with the $g' - V$ as a function of $B - V$ relation.

3.1 $g' - V$ as a Function of $B - V$ Relation

Fig. 5, Fig. 6, Fig. 7, and Fig. 8 show (a) $g' - V$ as a function of $B - V$ transformations for NIMIQ-1 (25740) (blue squares), SPACEWAY-3 (32018) (green circles), SES-2 (37809) (red diamonds), and NIMIQ-6 (38342) (magenta triangles), respectively, with our observed data and satellite transformation (fit, colored solid line), the astronomical transformation of [20] (black dashed line), and the solar color index (orange solid vertical line) from [39], (b) the difference (delta) between the observed data and the satellite transformation (color symbols), and (c) the difference (delta) between the observed data and the astronomical transformation (black symbols). The error bars for the observed data are also shown.

The title of (a) contains the equation of the linear fit (transformation) determined for the observed data with the one-sigma error (1σ) in the slope and y-intercept. We use this error in the slope and y-intercept to compare the satellite transformation to that of the astronomical transformation and determine if they are comparable within the error of the satellite transformation. The linear fit is not weighted by the error bars. The least squares linear fit to the observed data was determined using NumPy[3] version 1.13.3 module 'polyfit'.

The RMS of the observed data about the fit is given [40], and the sample coefficient of determination (r^2) or squared sample correlation coefficient (r) is also provided. As a qualitative description in our analysis we will refer to the range

[3] http://www.numpy.org/

of RMS ≤ 0.03 mag as small, 0.03 < RMS < 0.05 mag as moderate, and RMS ≥ 0.05 mag as large. We will also use this same description and range when referring to the difference between the observed data and the transformations in (b) and (c). The sample correlation coefficient was determined using NumPy's module 'corrcoef'. The coefficient of determination expresses the proportion of the total variation in the values of the y-axis data that may be explained by a linear relationship with the values of the x-axis data. A coefficient of determination of say 0.25 means that 25% of the total variation of the values of y-axis data in our sample is accounted for by a linear relationship with the values of the x-axis data [41]. The coefficient of determination, r^2, can take on values from 0 to 1, with $r^2 = 0$ implying that the observed data is completely uncorrelated with the line, and $r^2 = 1$ implying the observed data is a perfect fit to the line. We use a value for the coefficient of determination of $r^2 = 0.25$ as an estimate to determine whether it is valid for the observed data to be represented by the linear fit. Linear fits with $r^2 < 0.25$ are not a valid representation of the observed data and $r^2 \geq 0.25$ are valid representations of the observed data. As a qualitative description in our analysis we will refer to the range of $r^2 < 0.25$ as a poor fit, $0.25 \leq r^2 \leq 0.75$ as a good fit, and $r^2 > 0.75$ as a great fit. Transformations that are a poor fit to the observed data are viewed as invalid, so we do not provide a detailed analysis. Panels (b) and (c) are useful to provide an estimate of what errors one may obtain if using our derived satellite transformation or the astronomical transformation.

Fig. 9 shows $g' - V$ as a function of $B - V$ of each satellite plotted together with their observed data and transformation, the astronomical transformation of [20] (black dashed line), and the solar color index (orange solid vertical line). This shows how all of the transformations for each satellite compare to each other. This demonstrates the span of color index for each satellite on the x-axis and y-axis, how they compare to each other, and how each compares to all of the satellites as a whole.

Fig. 10 shows (a) $g' - V$ as a function of $B - V$ transformation for all of the satellites with our observed data (gray hexagons) and total satellite transformation (gray solid line), the astronomical transformation of [20] (black dashed line), and the solar color index (orange solid vertical line), (b) the difference between the observed data and satellite transformation, and (c) the difference between the observed data and the astronomical transformation. The error bars for the observed data are also shown.

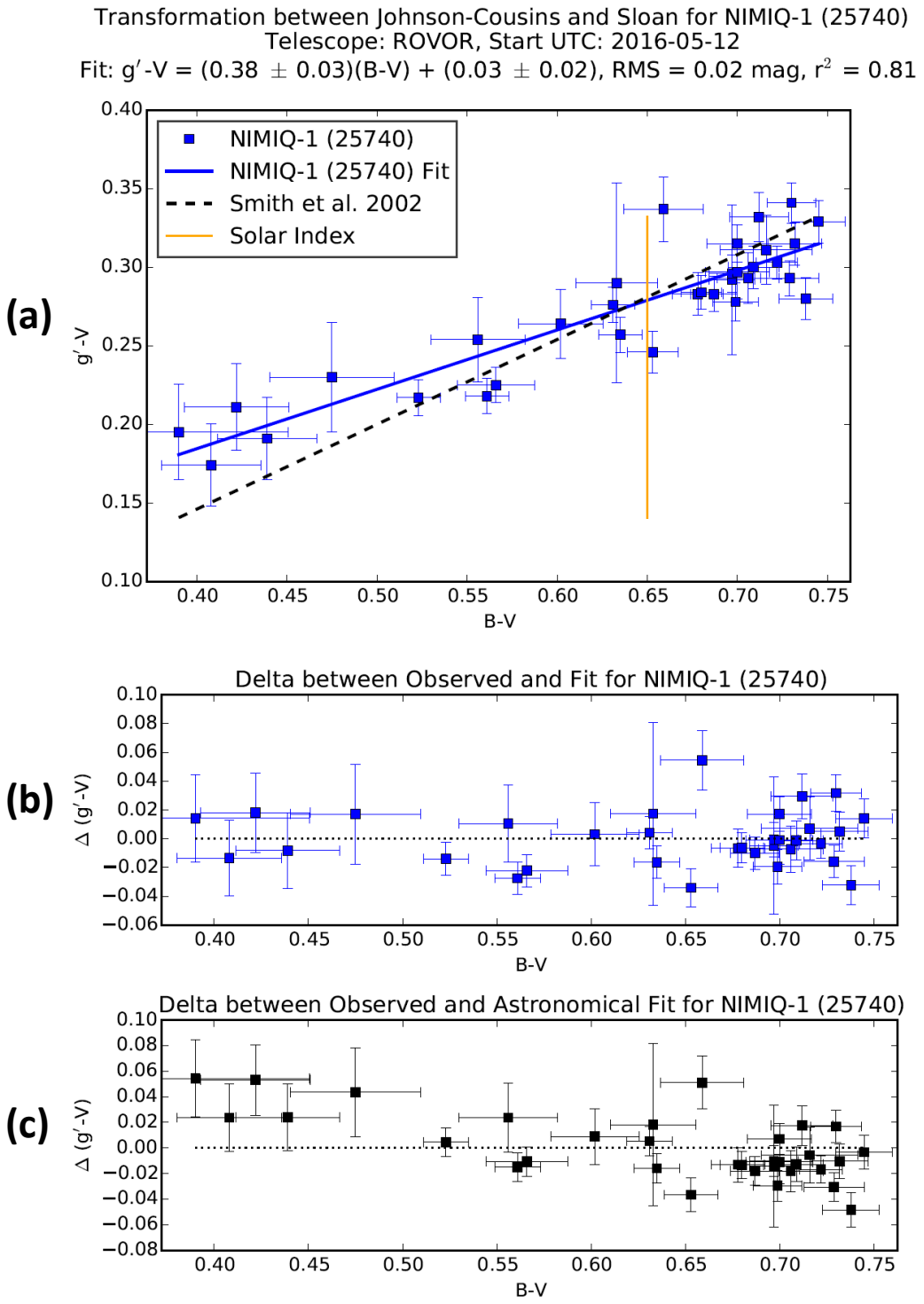

Fig. 5. (a) $g' - V$ as a function of $B - V$ transformations for NIMIQ-1 (25740) with our observed data and fit, the astronomical transformation of [20], and the solar color index, (b) the difference between the observed data and our fit, and (c) the difference between the observed data and the astronomical transformation.

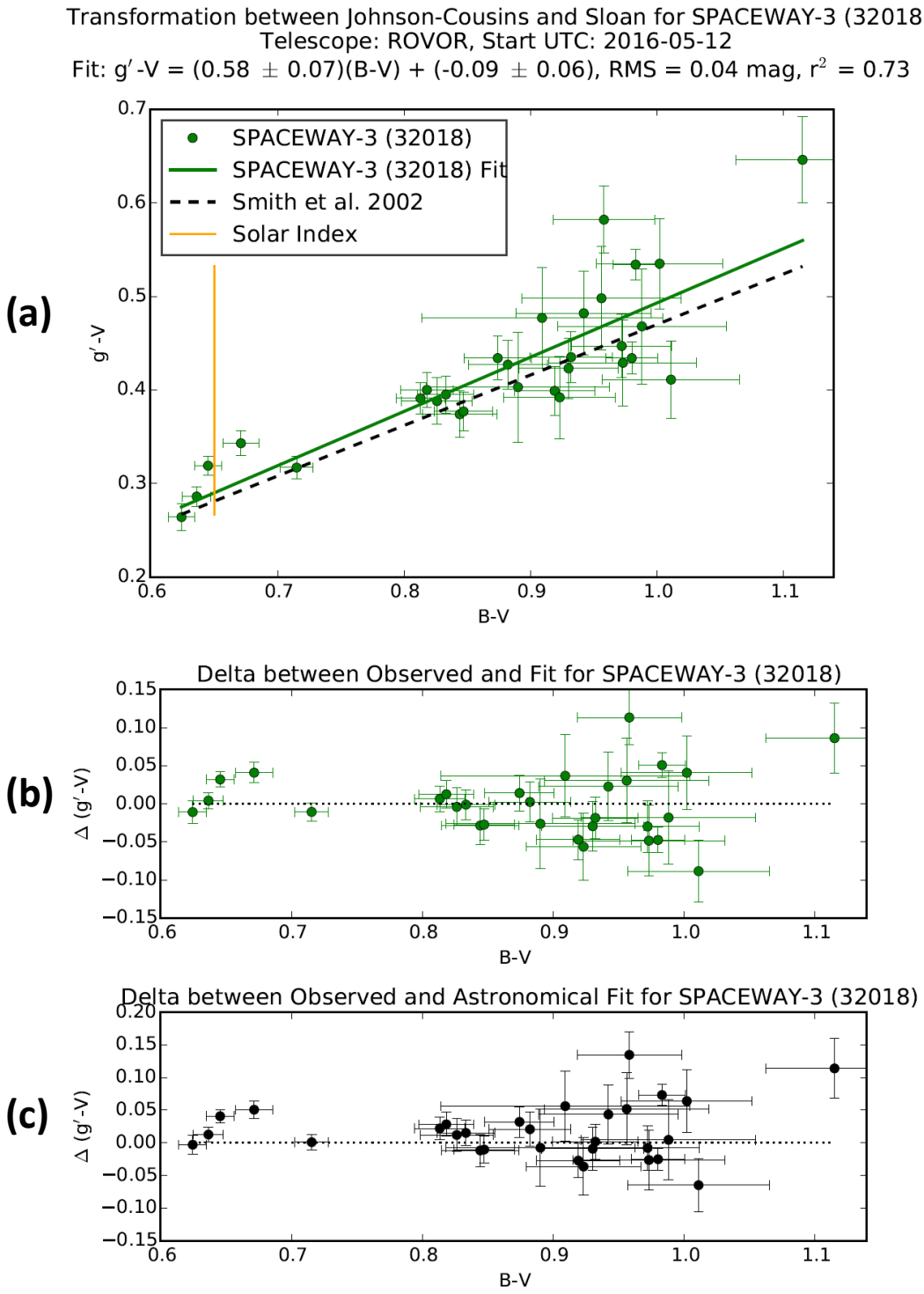

Fig. 6. (a) $g' - V$ as a function of $B - V$ transformations for SPACEWAY-3 (32018) with our observed data and fit, the astronomical transformation of [20], and the solar color index, (b) the difference between the observed data and our fit, and (c) the difference between the observed data and the astronomical transformation.

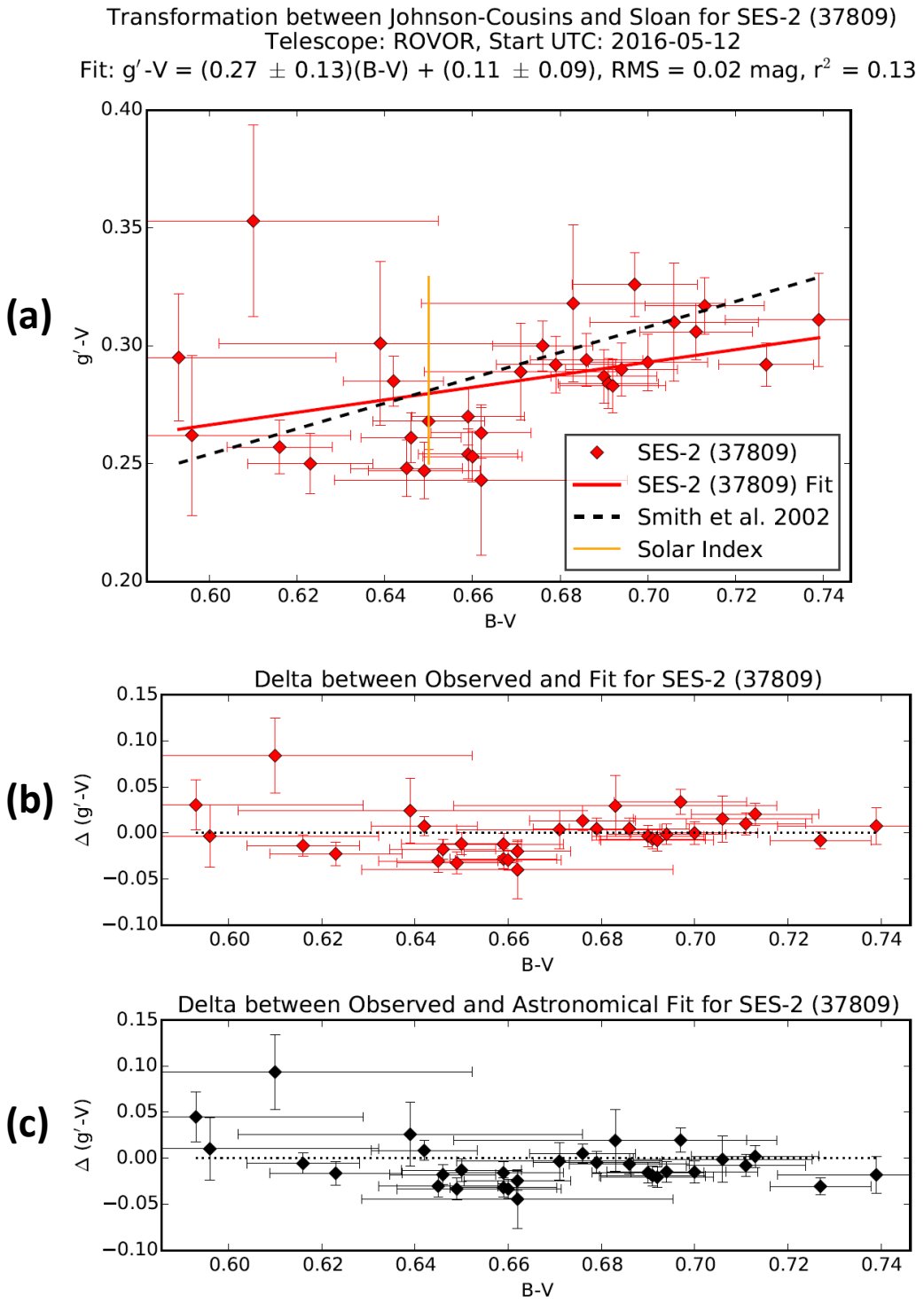

Fig. 7. (a) $g' - V$ as a function of $B - V$ transformations for SES-2 (37809) with our observed data and fit, the astronomical transformation of [20], and the solar color index, (b) the difference between the observed data and our fit, and (c) the difference between the observed data and the astronomical transformation.

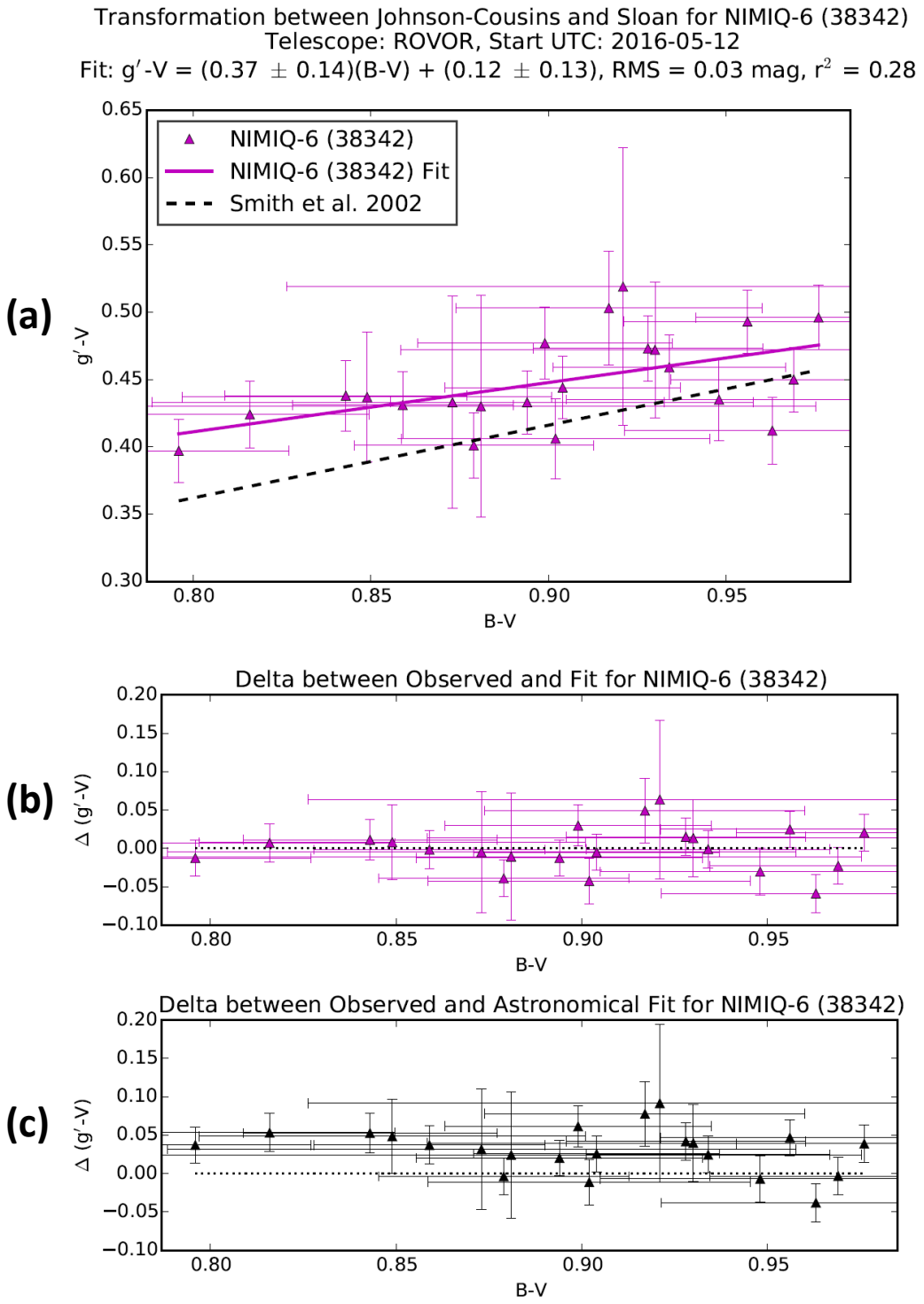

Fig. 8. (a) $g' - V$ as a function of $B - V$ transformations for NIMIQ-6 (38342) with our observed data and fit, the astronomical transformation of [20], and the solar color index, (b) the difference between the observed data and our fit, and (c) the difference between the observed data and the astronomical transformation.

Fig. 5 shows the transformation for NIMIQ-1 (25740). The observed data is a good fit to the linear transformation as seen in panel (a), with the satellite transformation intersecting the astronomical transformation, but with a different slope. The RMS about the fit is small. The satellite transformation is distinctly different (outside of three sigma, 3σ) than that of the astronomical transformation. The linear fit is influenced by the blue data points from a $B - V$ of 0.4 to 0.5 mag. If the data were collected during glint season and the observed data took on even bluer color indices, it is possible the derived transformation would deviate even more from the astronomical transformation for this satellite. Note that the satellite transformation intersects with the astronomical transformation at the solar color index. In panel (b), the difference between the observed data and the satellite transformation is in general small for most of the observed data, but is as large as about 0.05 mag. The difference between the observed data and the astronomical transformation is similar but slightly larger, as seen in panel (c).

Fig. 6 shows the transformation for SPACEWAY-3 (32018). The observed data is a good fit to the linear transformation, although not intersecting the astronomical transformation, but close to it. The RMS is moderate. The satellite transformation within one sigma is comparable to the astronomical transformation. The difference between the observed data and the satellite transformation is large, up to about 0.1 mag for some of the data, while it is slightly larger for the astronomical transformation.

Fig. 7 shows the transformation for SES-2 (37809). The observed data is a poor fit to the linear transformation. For this object's observed data the span along the x-axis ($B - V$) throughout the night is small, about 0.15 mag. Due to this and the precision of the data along the y-axis ($g' - V$) it is not surprising that a poor fit to the data is obtained. Curiously, we note that the satellite transformation intersects with the astronomical transformation at the solar color index, just like NIMIQ-1 (25740), even as a poor fit to the observed data.

Fig. 8 shows the transformation for NIMIQ-6 (38342). The observed data is a good fit to the linear transformation, not intersecting the astronomical transformation, but near it with a similar slope. The RMS is small. The satellite transformation within two sigma is comparable to the astronomical transformation. The difference between the observed data and our transformation is large, with some data at or larger than 0.05 mag away from the fit, while it is even larger for the astronomical fit. Lastly, we note that two of the four satellite transformations intersect with the astronomical transformation at the solar color index; the significance of this, if any, is unclear.

Fig. 9 shows the transformations for each of the satellites plotted on the same graph. The span of color index range for all of the satellites is much larger than for any individual satellite. Note that the color index range ($B - V$) spanned by SES-2 (37809) is small compared to the other satellites, with NIMIQ-6 (38342) spanning a slightly larger range with an $r^2 = 0.28$, just above the value considered valid. The color index range of SPACEWAY-3 (32018) would be almost the same as NIMIQ-6 (38342) if not for the single redder data point that gives the satellite's data the larger span of color index. The valid individual satellite transformations appear to differ visually, but tend to overlap when in similar $B - V$ space. The individual satellite transformations extrapolated outside of the observed $B - V$ data range would result in significant differences; therefore, transformations should not be extrapolated outside of the color index range from which they were derived.

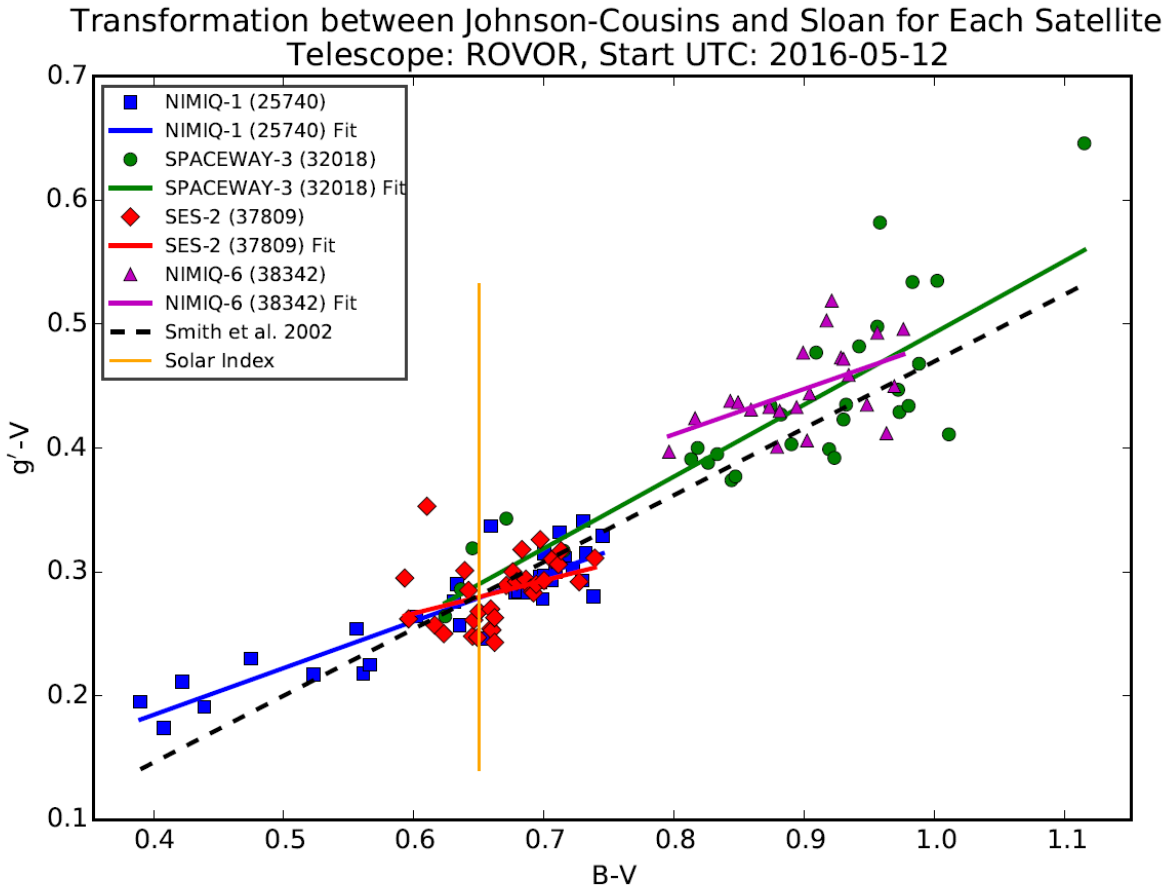

Fig. 9. $g' - V$ as a function of $B - V$ transformations of each satellite with the observed data and fit, the astronomical transformation of [20], and the solar color index.

Fig. 10 shows the transformation determined using the data collected from all of the satellites together, called the total satellite transformation. The observed data is a great fit to the linear transformation, with the satellite transformation going through the astronomical transformation with a slightly differing slope. The RMS about the transformation is small. Our transformation within three sigma is comparable to the astronomical transformation. The difference between the observed data and satellite transformation is large, with some differences as large as 0.05 to 0.1 mag. The differences for the astronomical transformation are comparable with the satellite transformation although slightly larger.

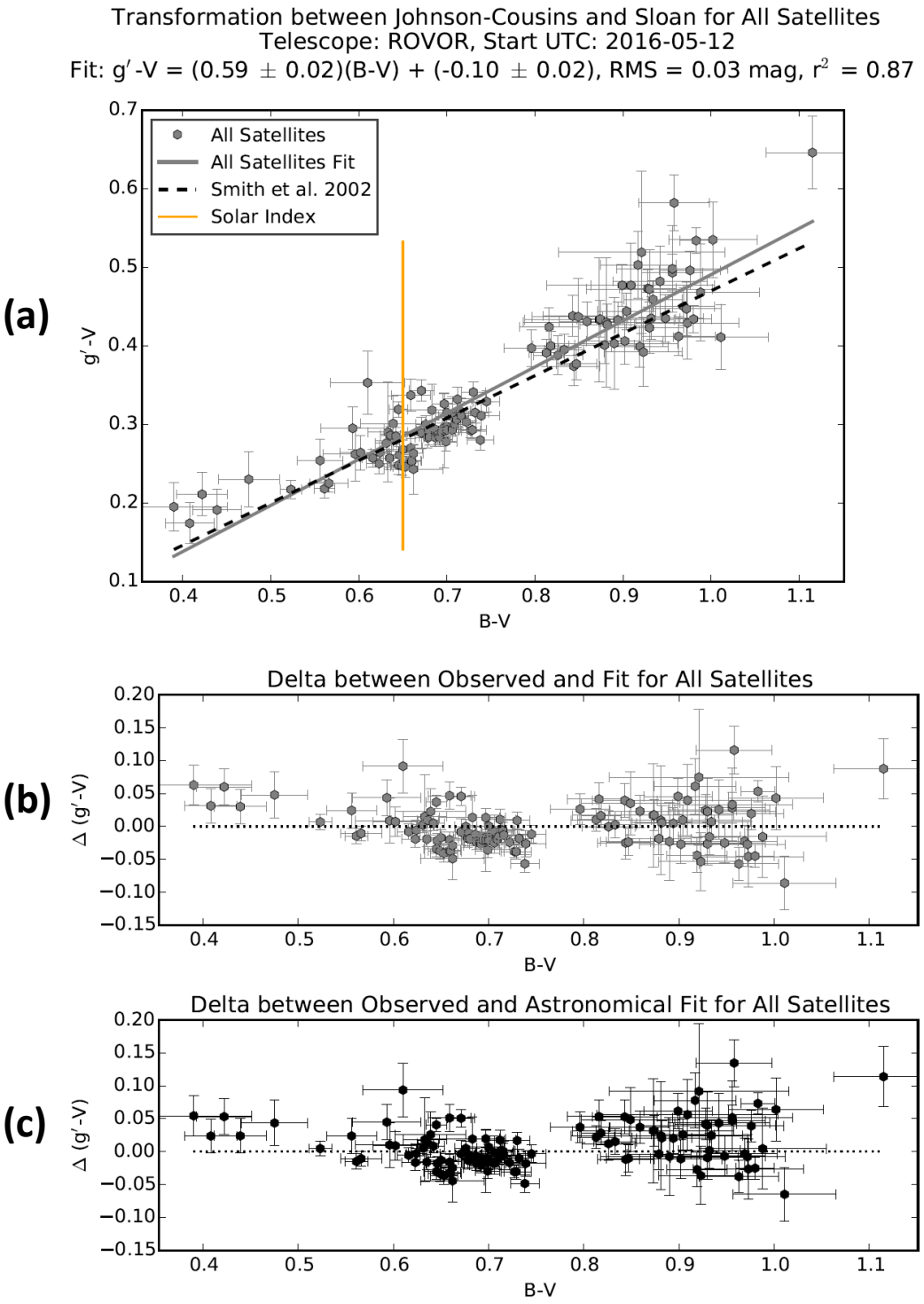

Fig. 10. (a) $g' - V$ as a function of $B - V$ transformation for all of the satellites with our observed data and fit, the astronomical transformation of [20], and the solar color index, (b) the difference between the observed data and our fit, and (c) the difference between the observed data and the astronomical transformation.

Tab. 5 shows a summary of the $g' - V$ as a function of $B - V$ relation. It appears that this relation provides a valid fit with small RMS for the total satellite transformation based on the small sample analyzed here, but is only within three sigma of the astronomical transformation. Of the valid individual satellite transformations, one of the transformations is not comparable to the astronomical transformation while two are comparable; the individual satellite transformations are disparate. With the total satellite transformation being comparable to the astronomical transformation, there is an inconsistency between the individual satellite transformation and the total satellite transformation.

Tab. 5. Summary of the $g' - V$ as a function of $B - V$ relation.

Satellite	r^2	RMS (mag)	σ from Astronomical Transformation
NIMIQ-1 (25740)	0.81 (great fit)	0.02	> 3 (distinct)
SPACEWAY-3 (32018)	0.73 (good fit)	0.04	< 1
SES-2 (37809)	0.13 (poor fit)	…	…
NIMIQ-6 (38342)	0.28 (good fit)	0.03	< 2
All	0.87 (great fit)	0.03	< 3

3.2 $r' - V$ as a Function of $B - V$ Relation

Fig. 11, Fig. 12, Fig. 13, and Fig. 14 show the transformations for NIMIQ-1 (25740), SPACEWAY-3 (32018), SES-2 (37809), and NIMIQ-6 (38342), respectively. All of the satellite transformations are poor fits, three with a coefficient of determination (r^2) of zero and the other slightly above zero. None of the observed data conforms to a linear relationship.

Fig. 15 shows the observed data and all of the transformations for each satellite. This shows that the observed data for each satellite represents a clump of data, from this view, it is clear that the observed data for each satellite indeed does not conform to a linear fit.

Fig. 16 shows the total satellite transformation. The linear fit to the observed data is good, with $r^2 = 0.53$, so that all of the observed data conforms to a linear relationship, whereas the individual satellites do not. The satellite transformation has a similar slope and is parallel to the astronomical transformation with the observed satellite data generally below the astronomical transformation. The RMS is large at 0.07 mag. The satellite transformation is comparable within two sigma to the astronomical transformation. When considering all of the satellite data, we get clumps of data from the individual satellites spanning a larger range of color index space that allows a linear fit to be achieved. However, the data contains a significant amount of scatter about the linear transformation, with differences between our observed data and the satellite transformation as large as 0.2 mag. The differences between the observed data and the astronomical transformation are even larger due to the shift between the two transformations, with values almost as large as 0.3 mag.

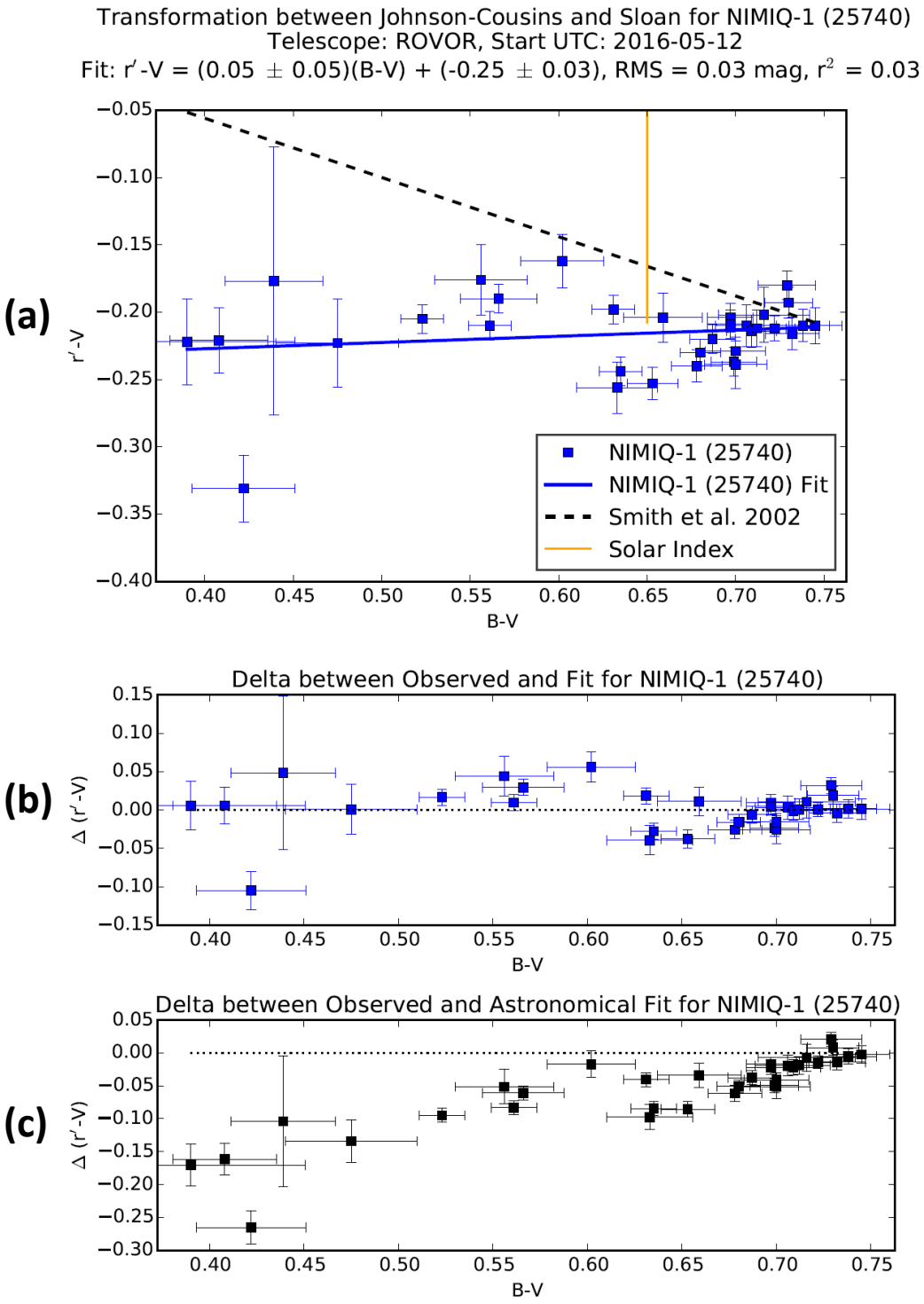

Fig. 11. (a) $r' - V$ as a function of $B - V$ transformations for NIMIQ-1 (25740) with our observed data and fit, the astronomical transformation of [20], and the solar color index, (b) the difference between the observed data and our fit, and (c) the difference between the observed data and the astronomical transformation.

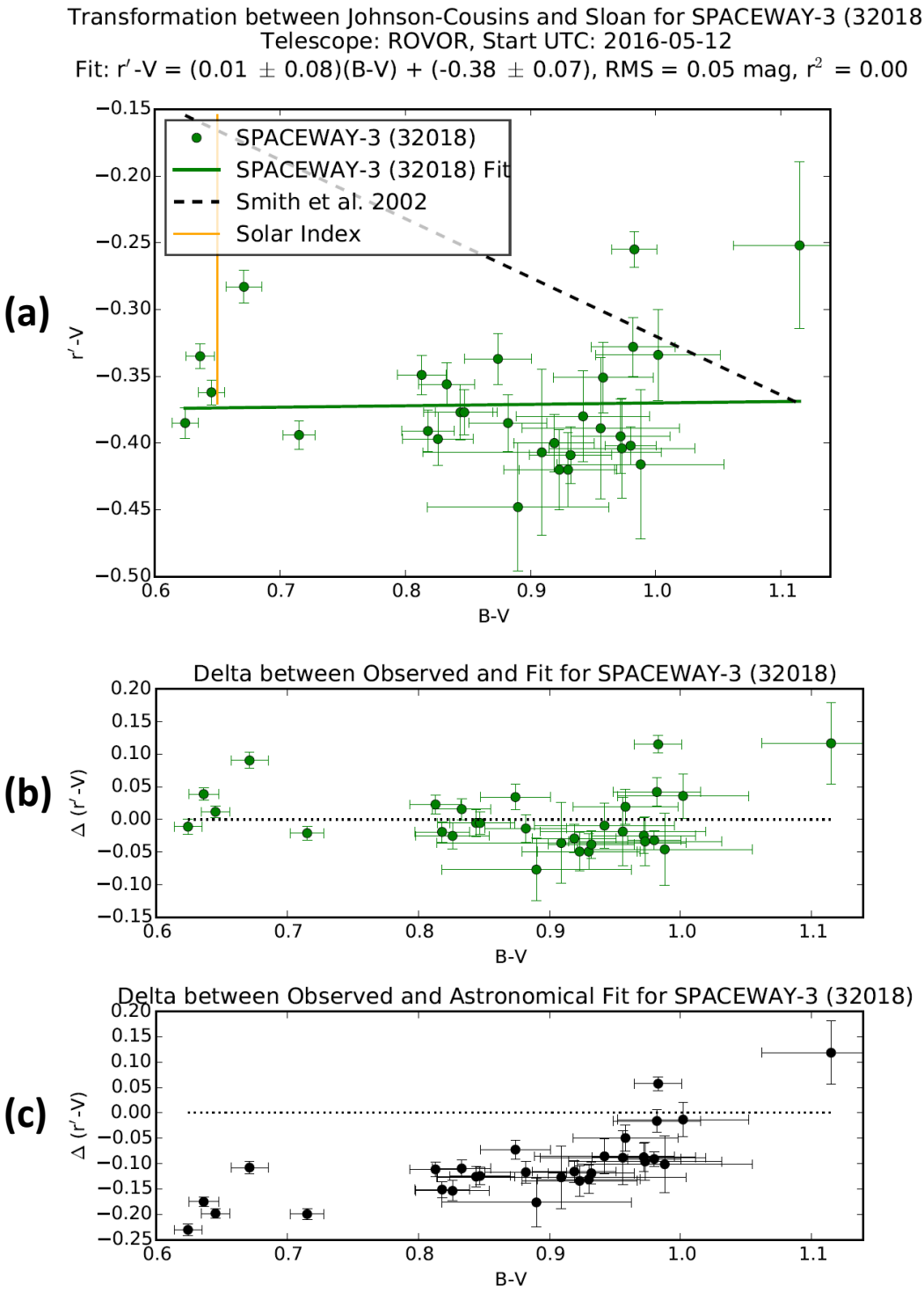

Fig. 12. (a) $r' - V$ as a function of $B - V$ transformations for SPACEWAY-3 (32018) with our observed data and fit, the astronomical transformation of [20], and the solar color index, (b) the difference between the observed data and our fit, and (c) the difference between the observed data and the astronomical transformation.

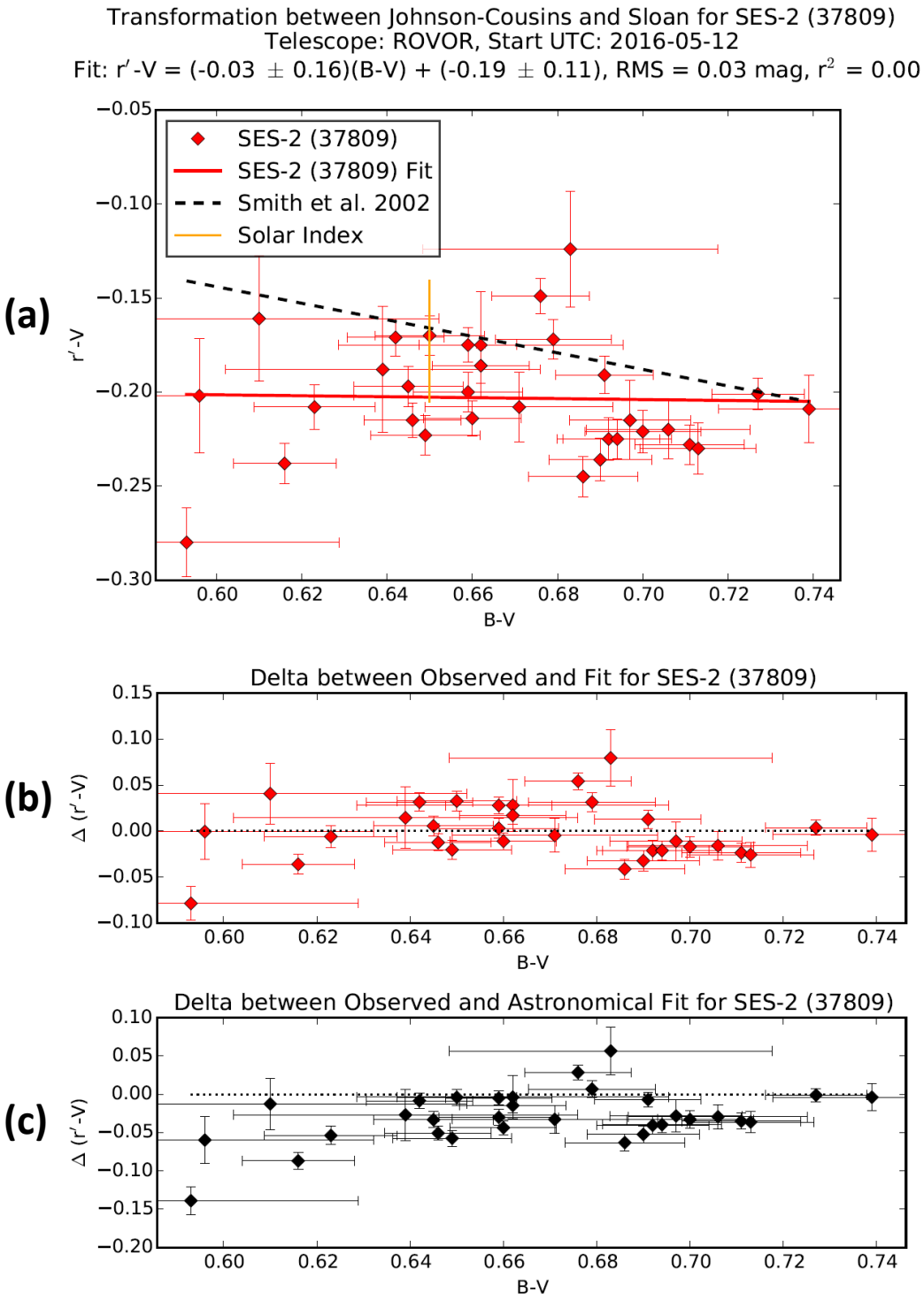

Fig. 13. (a) $r' - V$ as a function of $B - V$ transformations for SES-2 (37809) with our observed data and fit, the astronomical transformation of [20], and the solar color index, (b) the difference between the observed data and our fit, and (c) the difference between the observed data and the astronomical transformation.

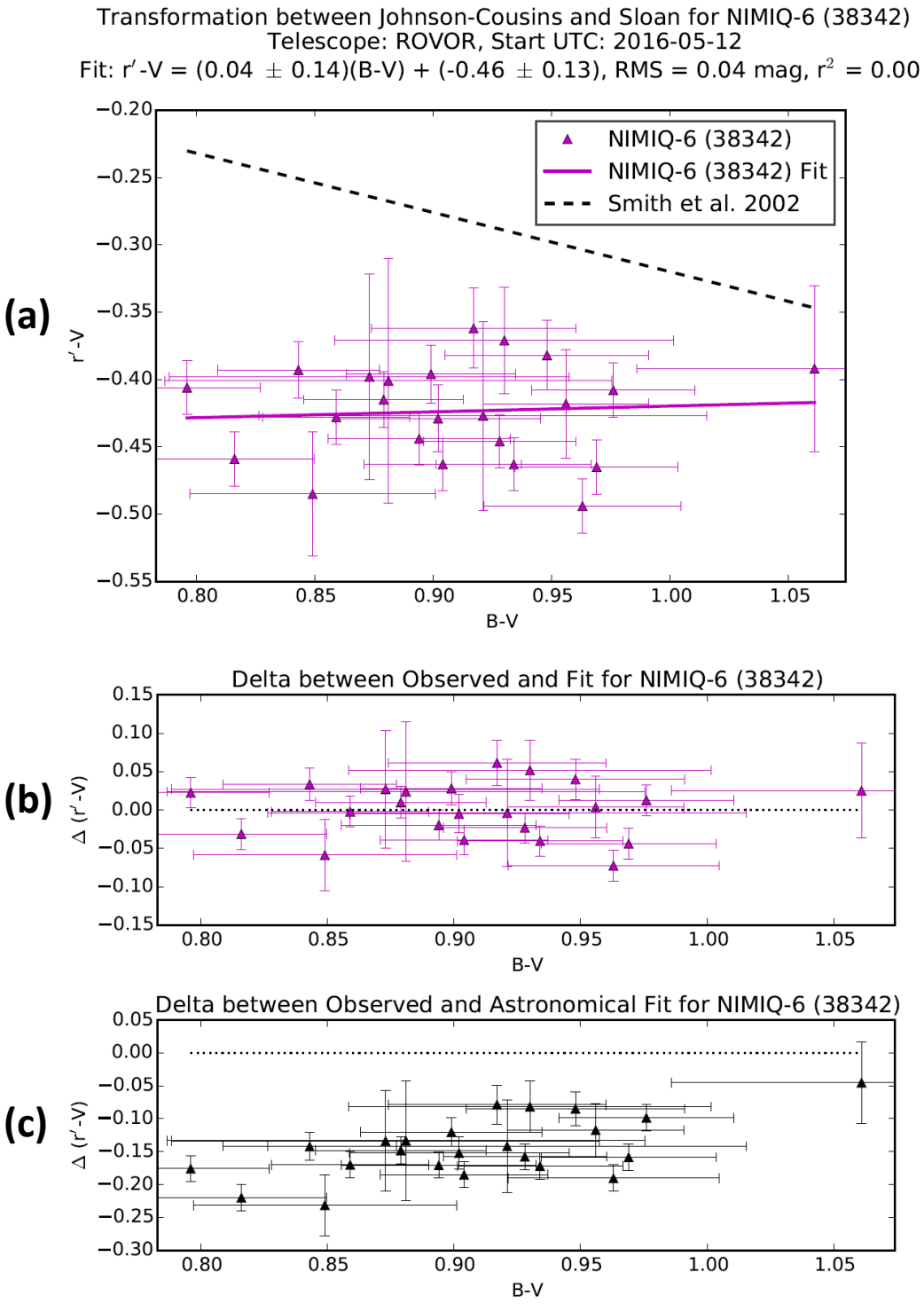

Fig. 14. (a) $r' - V$ as a function of $B - V$ transformations for NIMIQ-6 (38342) with our observed data and fit, the astronomical transformation of [20], and the solar color index, (b) the difference between the observed data and our fit, and (c) the difference between the observed data and the astronomical transformation.

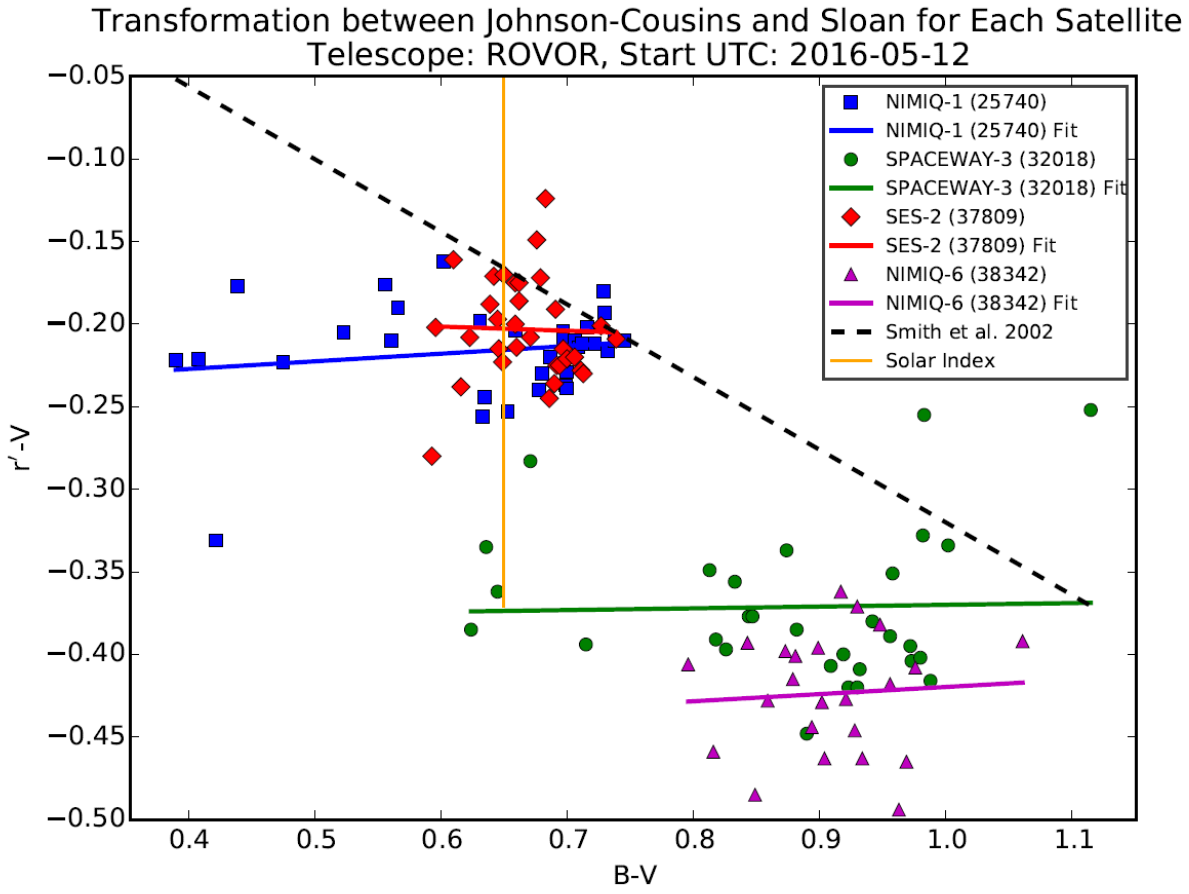

Fig. 15. $r' - V$ as a function of $B - V$ transformations of each satellite with the observed data and fit, the astronomical transformation of [20], and the solar color index.

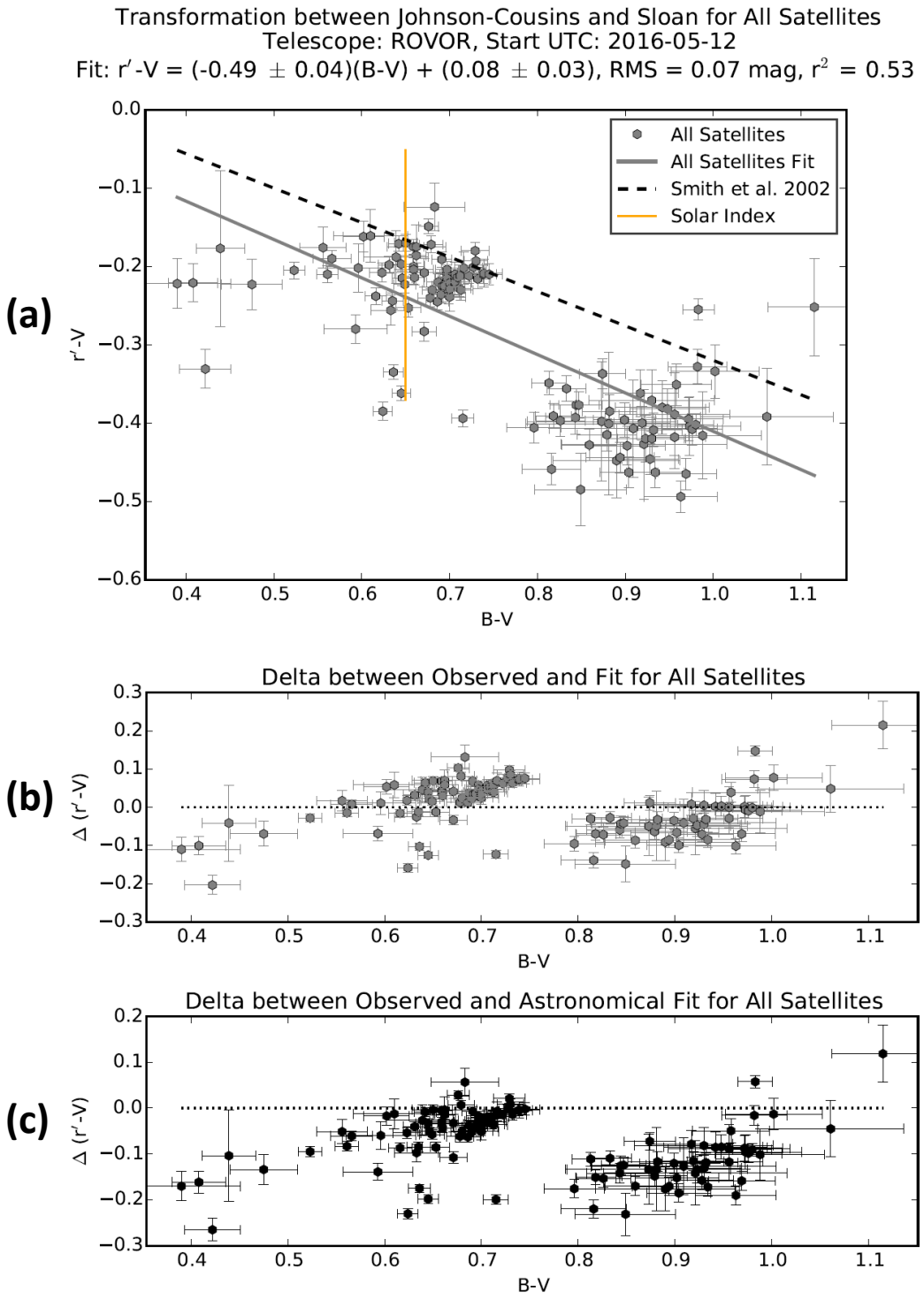

Fig. 16. (a) $r' - V$ as a function of $B - V$ transformation for all of the satellites with our observed data and fit, the astronomical transformation of [20], and the solar color index, (b) the difference between the observed data and our fit, and (c) the difference between the observed data and the astronomical transformation.

Tab. 6 shows a summary of the $r' - V$ as a function of $B - V$ relation. This relation provides a valid fit for all of the satellite data, but contains large scatter about this fit. The relation performs poorly for satellites on an individual basis with all of the individual satellite transformations invalid.

Tab. 6. Summary of the $r' - V$ as a function of $B - V$ relation.

Satellite	r^2	RMS (mag)	σ from Astronomical Transformation
NIMIQ-1 (25740)	0.03 (poor fit)	…	…
SPACEWAY-3 (32018)	0.00 (poor fit)	…	…
SES-2 (37809)	0.00 (poor fit)	…	…
NIMIQ-6 (38342)	0.00 (poor fit)	…	…
All	0.53 (good fit)	0.07	< 2

3.3 $r' - V$ as a Function of $V - R$ Relation

Fig. 17 shows the transformation for NIMIQ-1 (25740). The observed data is a poor fit to the linear transformation. Fig. 18 shows the transformation for SPACEWAY-3 (32018). The observed data is a good fit to the linear transformation, with the satellite transformation intersecting the astronomical transformation. The RMS scatter is small. The satellite transformation is comparable to the astronomical transformation within one sigma. The difference between the observed data and the transformation can be up to 0.05 mag and larger, while for the astronomical transformation it is similar.

Fig. 19 shows the transformation for SES-2 (37809). The observed data is a good fit to the linear transformation, with the transformation almost parallel to the astronomical transformation. The RMS is small. Our transformation is comparable to the astronomical transformation within one sigma. The difference between the observed data and our transformation can be large, with one data point off by 0.1 mag. The difference in the observed data and the astronomical transformation is comparable to our transformation.

Fig. 20 shows the transformation for NIMIQ-6 (38342). The observed data is a good fit to the linear transformation, with the satellite transformation intersecting the astronomical transformation. The RMS scatter is small. The satellite transformation is comparable within three sigma to the astronomical transformation. The difference between the observed data and the satellite transformation is large at around 0.05 mag, and slightly larger for the astronomical transformation.

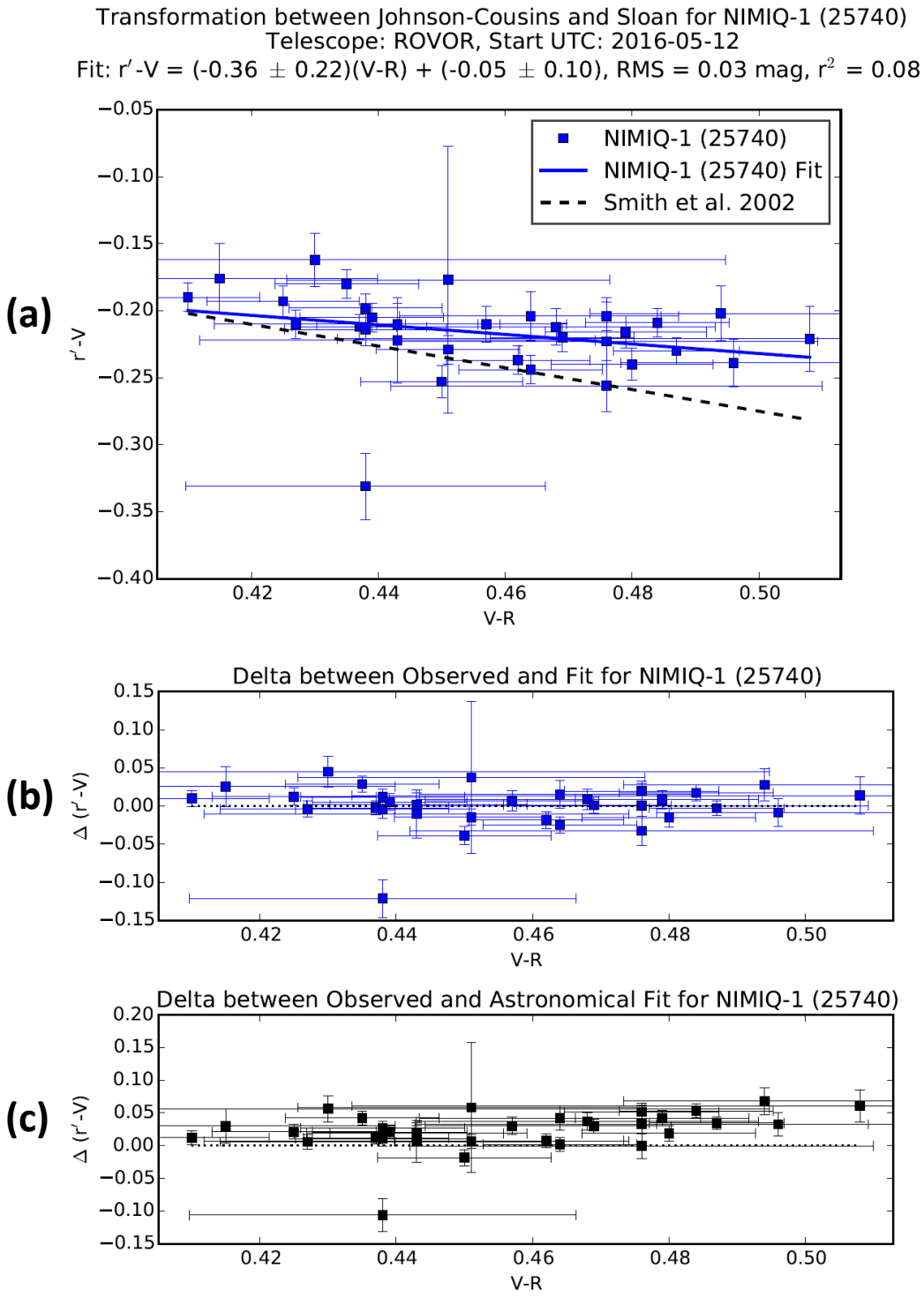

Fig. 17. (a) $r' - V$ as a function of $V - R$ transformations for NIMIQ-1 (25740) with our observed data and fit, the astronomical transformation of [20], and the solar color index, (b) the difference between the observed data and our fit, and (c) the difference between the observed data and the astronomical transformation.

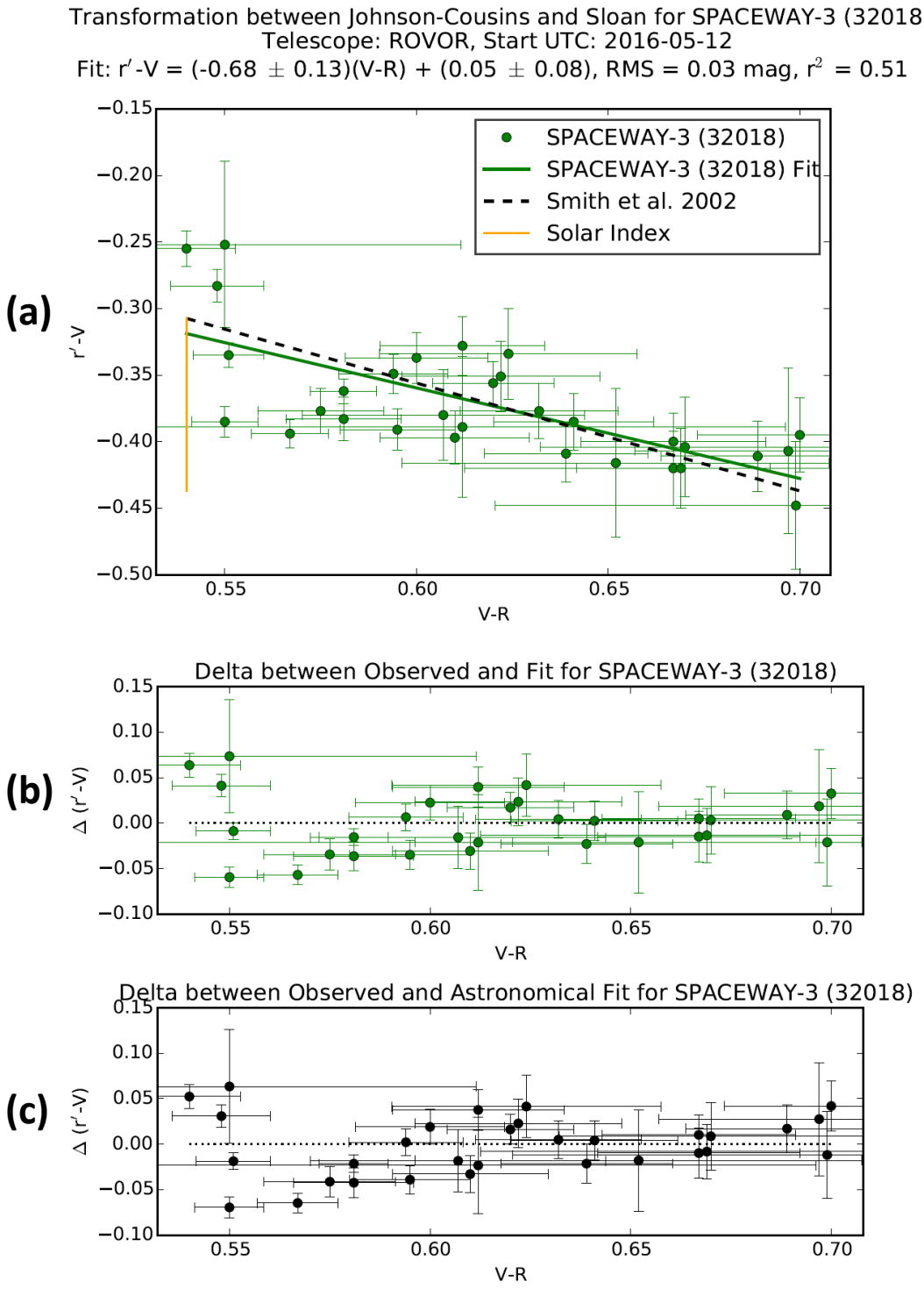

Fig. 18. (a) $r' - V$ as a function of $V - R$ transformations for SPACEWAY-3 (32018) with our observed data and fit, the astronomical transformation of [20], and the solar color index, (b) the difference between the observed data and our fit, and (c) the difference between the observed data and the astronomical transformation.

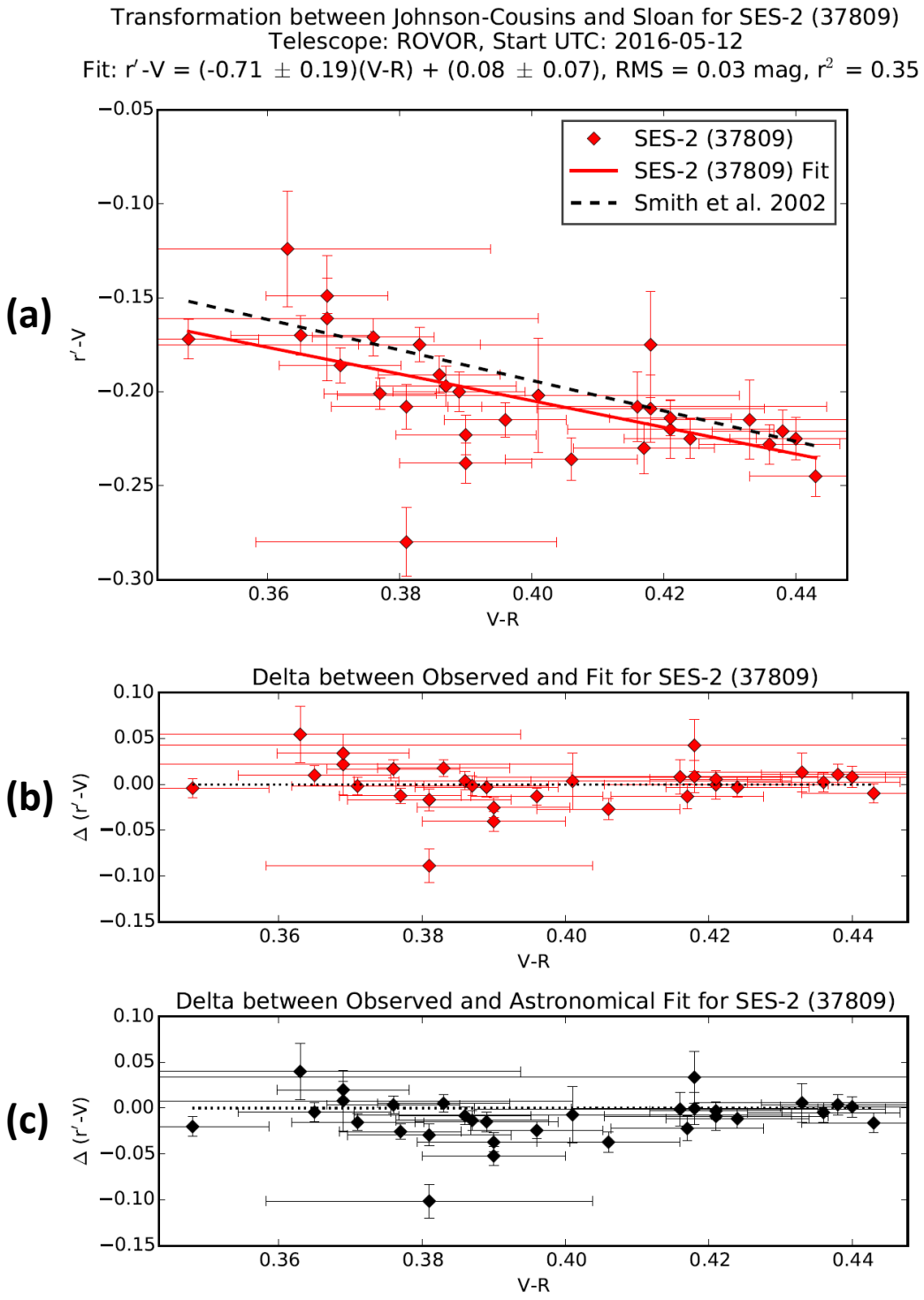

Fig. 19. (a) $r' - V$ as a function of $V - R$ transformations for SES-2 (37809) with our observed data and fit, the astronomical transformation of [20], and the solar color index, (b) the difference between the observed data and our fit, and (c) the difference between the observed data and the astronomical transformation.

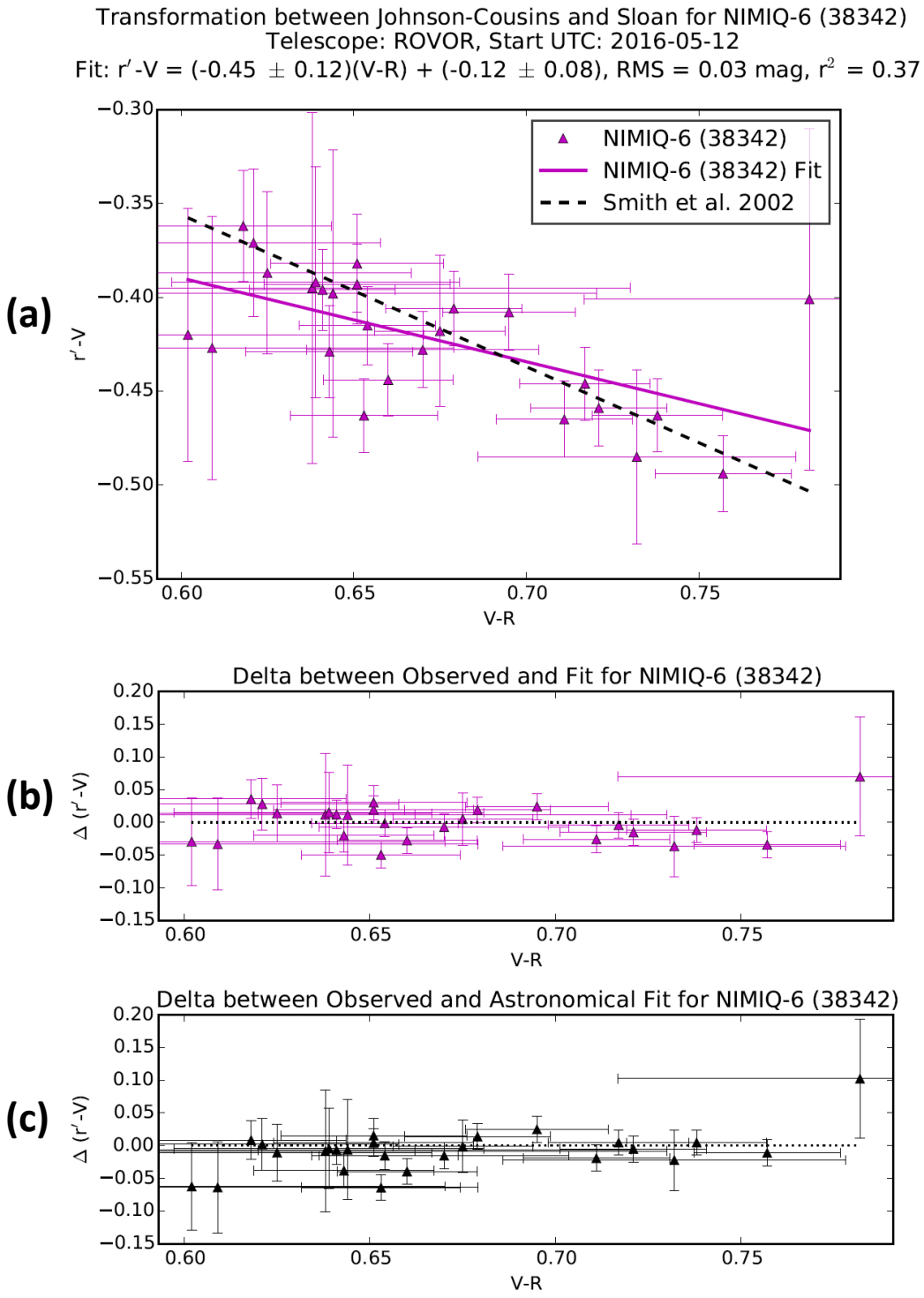

Fig. 20. (a) $r' - V$ as a function of $V - R$ transformations for NIMIQ-6 (38342) with our observed data and fit, the astronomical transformation of [20], and the solar color index, (b) the difference between the observed data and our fit, and (c) the difference between the observed data and the astronomical transformation.

Fig. 21 shows the transformations for each of the satellites together. NIMIQ-1 (25740) observed data lies above the astronomical transformation while SES-2 (37809) lies below the astronomical fit, both at the bluer color indices. Both SPACEWAY-3 (32018) and NIMIQ-6 (38342) are at the redder color indices, lying more or less along the astronomical transformation with the individual satellite transformations intersecting the astronomical transformation but with differing slopes for each. If we consider all of the satellite data, the color index range spanned is increased considerably compared to that for any individual satellite. The valid individual satellite transformations appear to be similar visually, except for NIMIQ-6 (38342) which may be due to a data point that is an outlier.

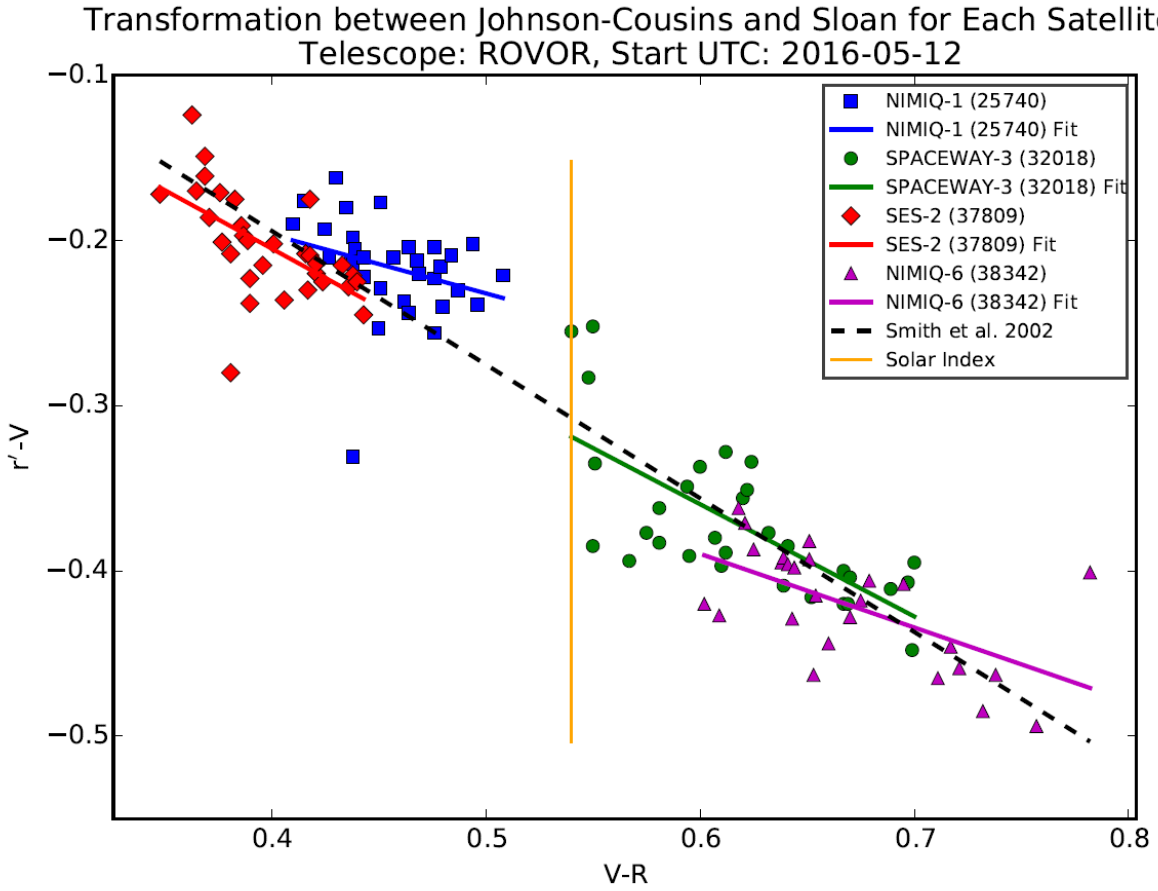

Fig. 21. $r' - V$ as a function of $V - R$ transformations of each satellite with the observed data and fit, the astronomical transformation of [20], and the solar color index.

Fig. 22 shows the total satellite transformation using all the satellites' data. The linear fit to the observed data is great at $r^2 = 0.89$ with a small RMS. The satellite transformation is extraordinarily similar to the astronomical transformation, essentially overlapping it. In fact, the satellite transformation and astronomical transformation equations are exactly the same. The differences between the observed data and the satellite and astronomical transformations for most of the data are up to 0.05 mag, with some of the data as large as 0.1 mag.

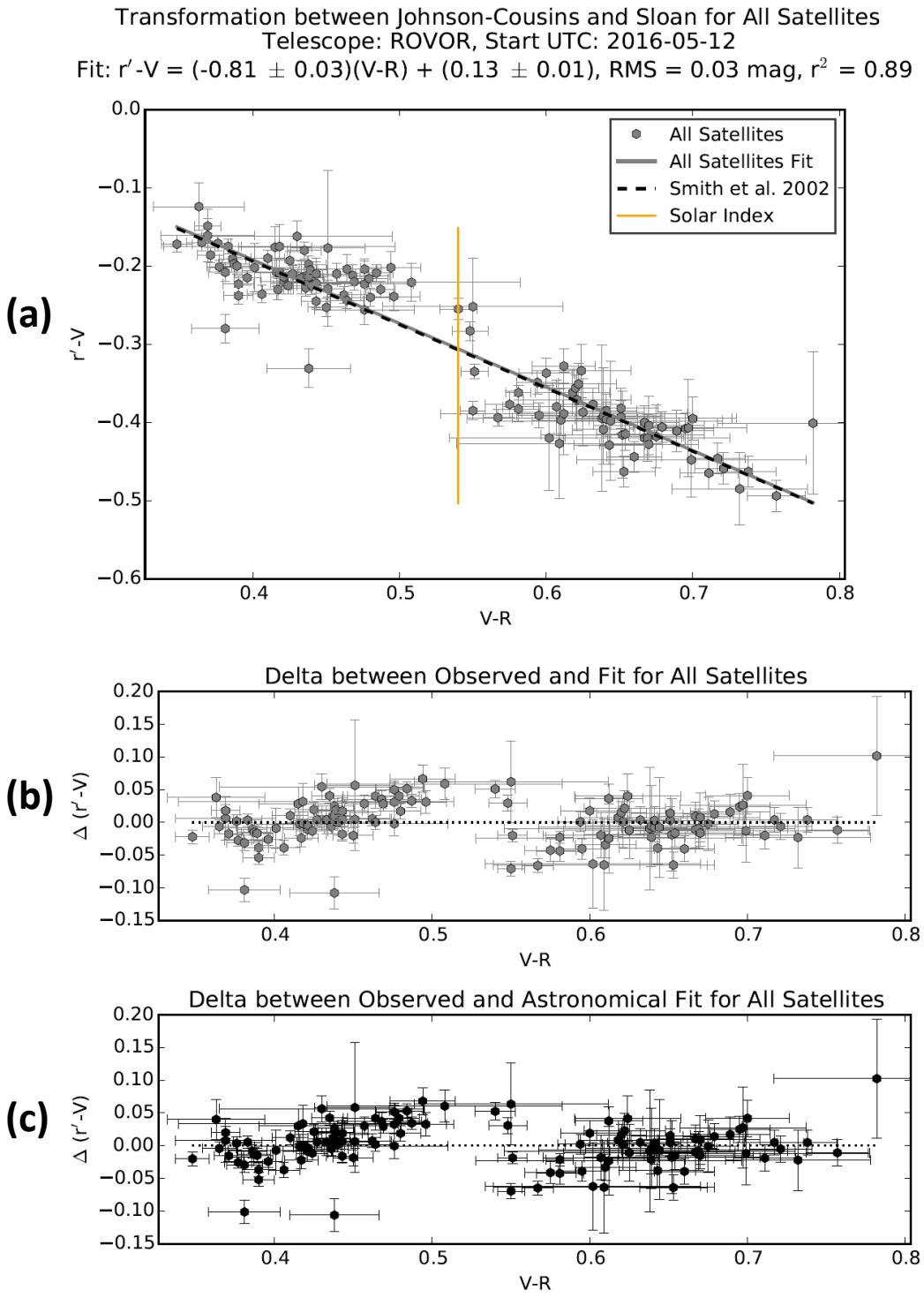

Fig. 22. (a) $r' - V$ as a function of $V - R$ transformation for all of the satellites with our observed data and fit, the astronomical transformation of [20], and the solar color index, (b) the difference between the observed data and our fit, and (c) the difference between the observed data and the astronomical transformation.

Tab. 7 shows a summary of the $r' - V$ as a function of $V - R$ relation. This relation provides a valid fit for satellites as a whole, based on the small sample analyzed here, with the total satellite transformation being exactly the same as the astronomical transformation for stars. With the three valid individual satellite transformations comparable to the astronomical transformation, the individual satellite transformations are consistent with each other and that of the total satellite transformation. In addition, all of the valid fits have small RMS. This relation appears to provide the best results so far.

Tab. 7. Summary of the $r' - V$ as a function of $V - R$ relation.

Satellite	r^2	RMS (mag)	σ from Astronomical Transformation
NIMIQ-1 (25740)	0.08 (poor fit)	…	…
SPACEWAY-3 (32018)	0.51 (good fit)	0.03	< 1
SES-2 (37809)	0.35 (good fit)	0.03	< 1
NIMIQ-6 (38342)	0.37 (good fit)	0.03	< 3
All	0.89 (great fit)	0.03	0, Exactly the Same

3.4 $g' - r'$ as a Function of $B - V$ Relation

Fig. 23 shows the transformation for NIMIQ-1 (25740). The observed data is a good fit to the linear transformation with the satellite transformation intersecting the astronomical transformation with a distinctly different slope. The RMS scatter is moderate. The satellite transformation is distinct (outside of three sigma) from the astronomical transformation. The difference between the observed data and the satellite transformation are mostly within 0.05 mag, but there are a few data points outside of this, with one larger than 0.1 mag. The difference between the observed data and the astronomical transformation is significantly worse. The difference is extreme at the blue color indices, around 0.3 mag, and smaller for the red color indices.

Fig. 24 shows the transformation for SPACEWAY-3 (32018). The observed data is a great fit to the linear transformation, with the satellite transformation above the astronomical transformation with a different slope. The RMS scatter is small. Our transformation is distinct (outside of three sigma) from the astronomical transformation. The difference between the observed data and satellite transformation is mostly within 0.05 mag with a few data points above this. The difference between the observed data and astronomical transformation is again significantly worse, with values up to 0.25 mag at the bluer color indices and generally smaller differences for the redder color indices where the difference is around zero.

Fig. 25 shows the transformation for SES-2 (37809). The observed data is a poor fit to the linear transformation. Fig. 26 shows the transformation for NIMIQ-6 (38342). The observed data is a poor fit to the linear transformation.

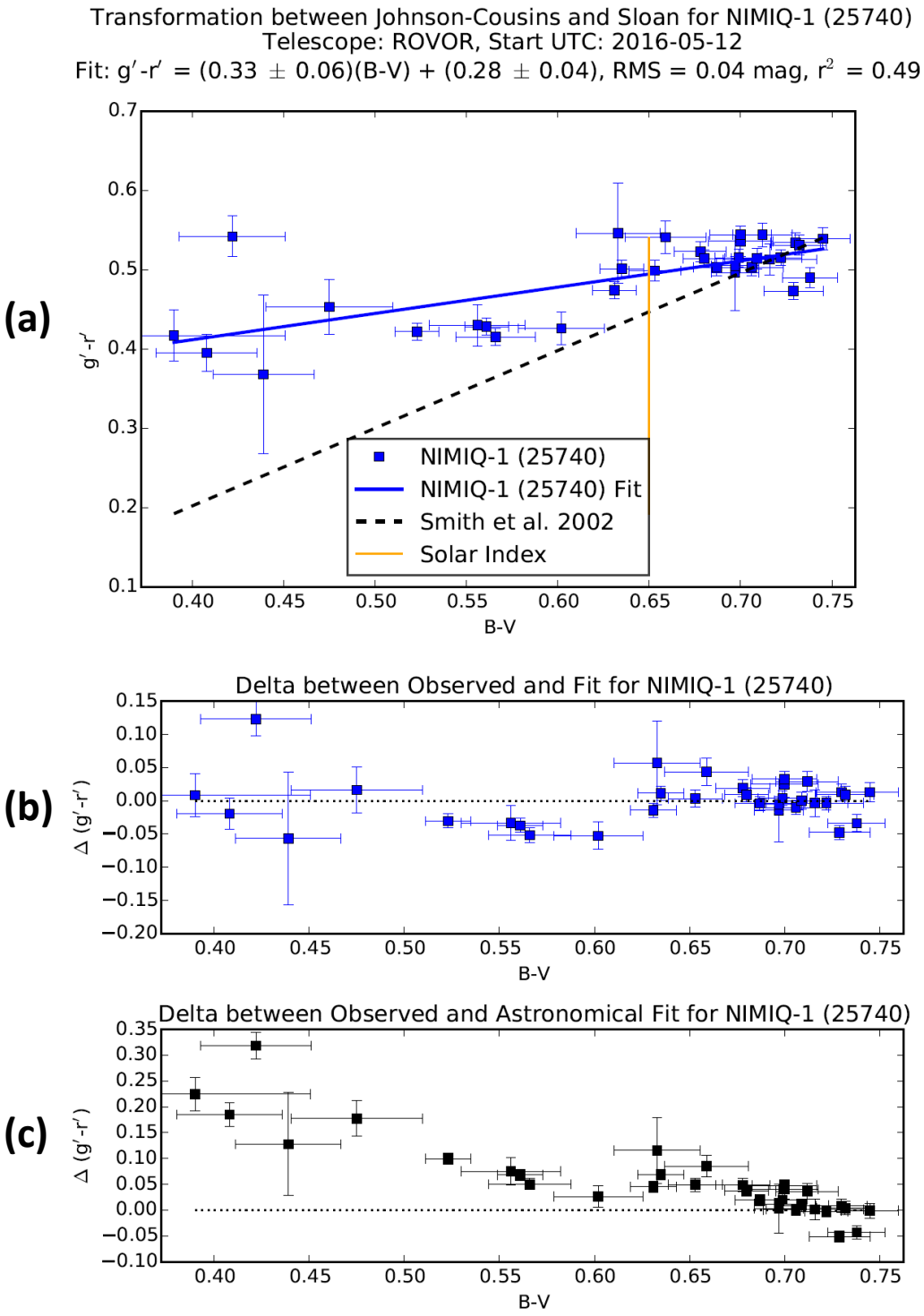

Fig. 23. (a) $g' - r'$ as a function of $B - V$ transformations for NIMIQ-1 (25740) with our observed data and fit, the astronomical transformation of [20], and the solar color index, (b) the difference between the observed data and our fit, and (c) the difference between the observed data and the astronomical transformation.

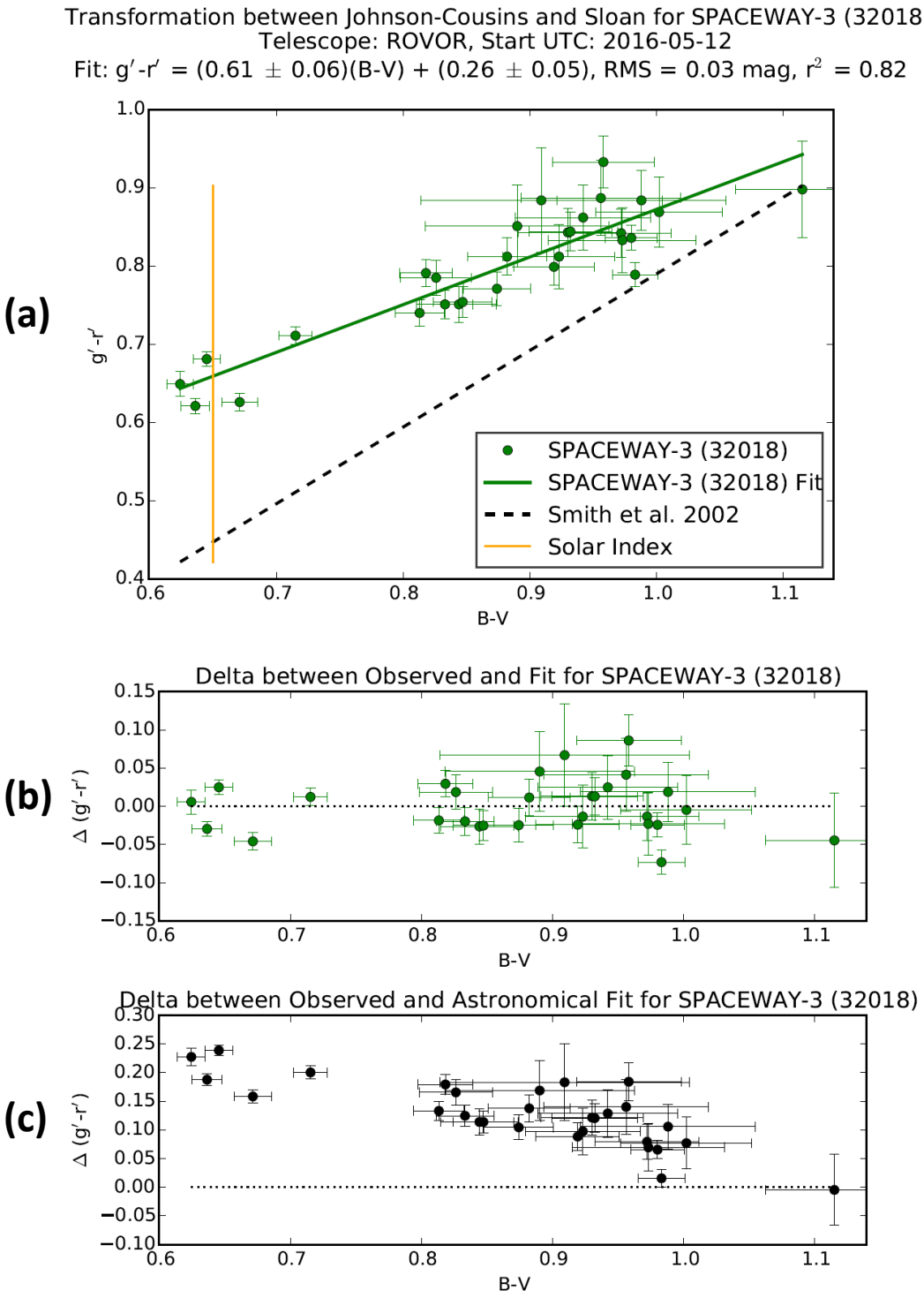

Fig. 24. (a) $g' - r'$ as a function of $B - V$ transformations for SPACEWAY-3 (32018) with our observed data and fit, the astronomical transformation of [20], and the solar color index, (b) the difference between the observed data and our fit, and (c) the difference between the observed data and the astronomical transformation.

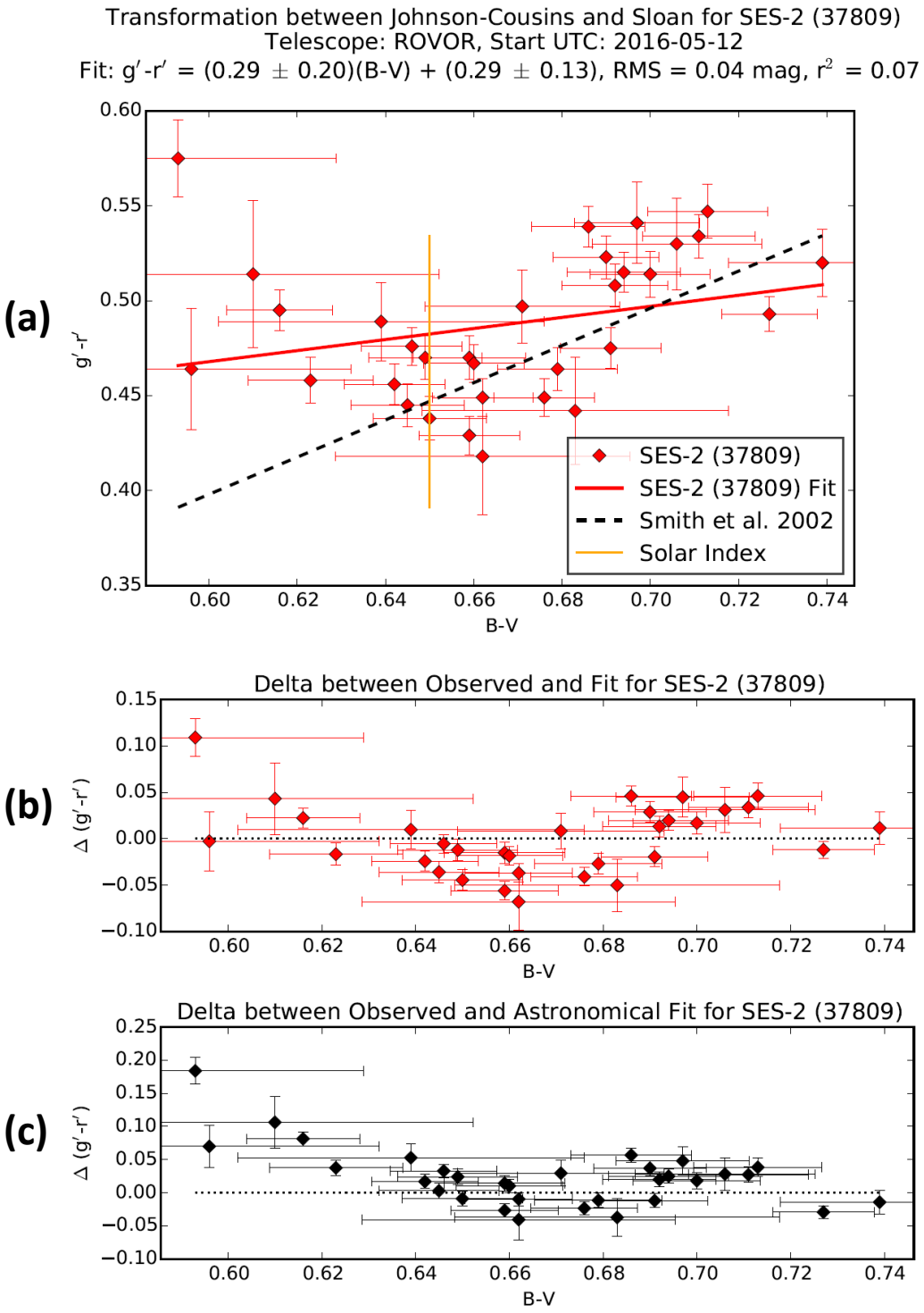

Fig. 25. (a) $g' - r'$ as a function of $B - V$ transformations for SES-2 (37809) with our observed data and fit, the astronomical transformation of [20], and the solar color index, (b) the difference between the observed data and our fit, and (c) the difference between the observed data and the astronomical transformation.

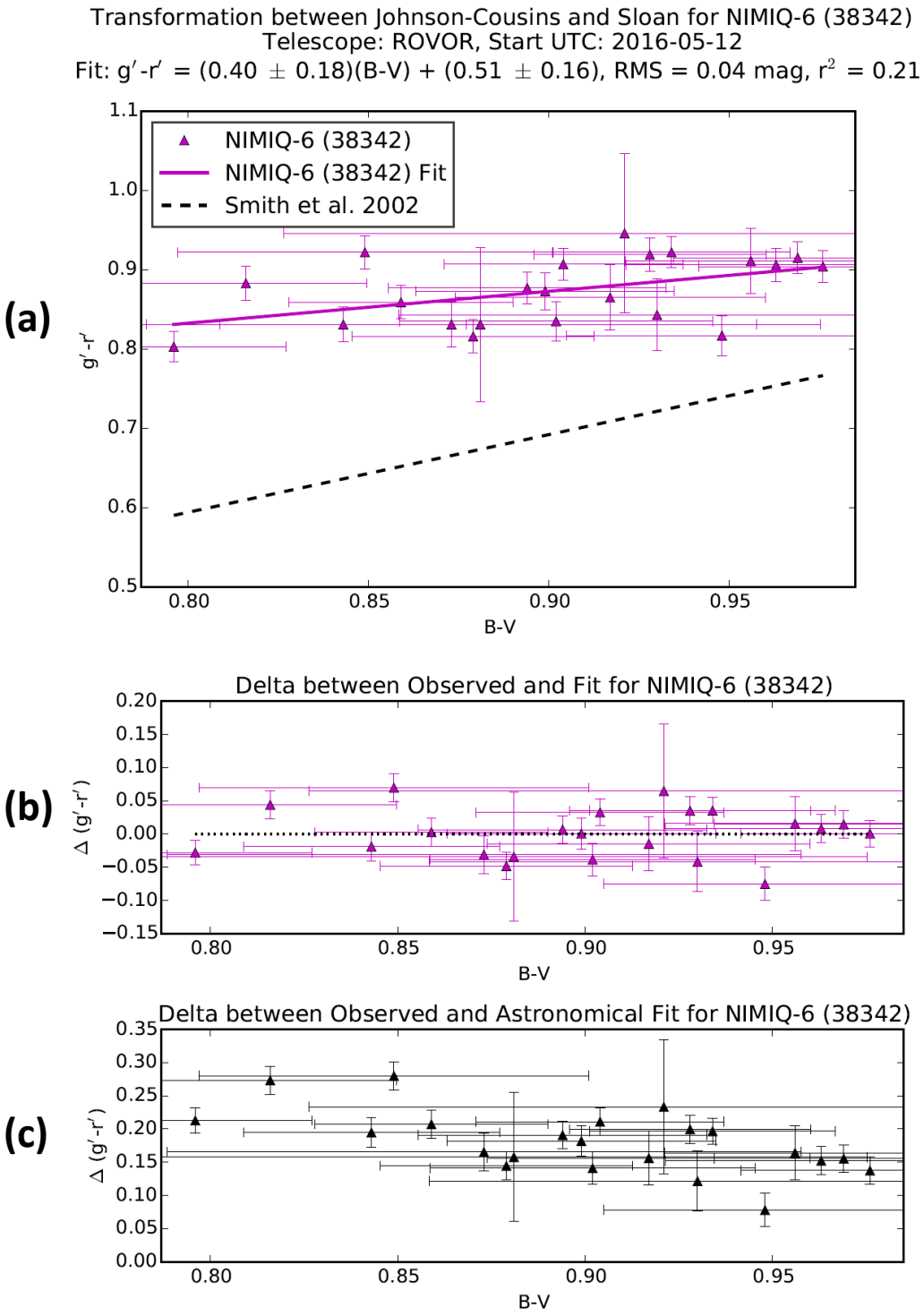

Fig. 26. (a) $g' - r'$ as a function of $B - V$ transformations for NIMIQ-6 (38342) with our observed data and fit, the astronomical transformation of [20], and the solar color index, (b) the difference between the observed data and our fit, and (c) the difference between the observed data and the astronomical transformation.

Fig. 27 shows the transformations for each of the satellites. NIMIQ-1 (25740) lies above the astronomical transformation and intersects with it, SES-2 (37809) observed data lies mostly around the astronomical transformation, while SPACEWAY-3 (32018) and NIMIQ-6 (38342) both lie above the astronomical transformation. The range of color indices spanned by all of the satellites is again significantly larger than that of the individual satellites.

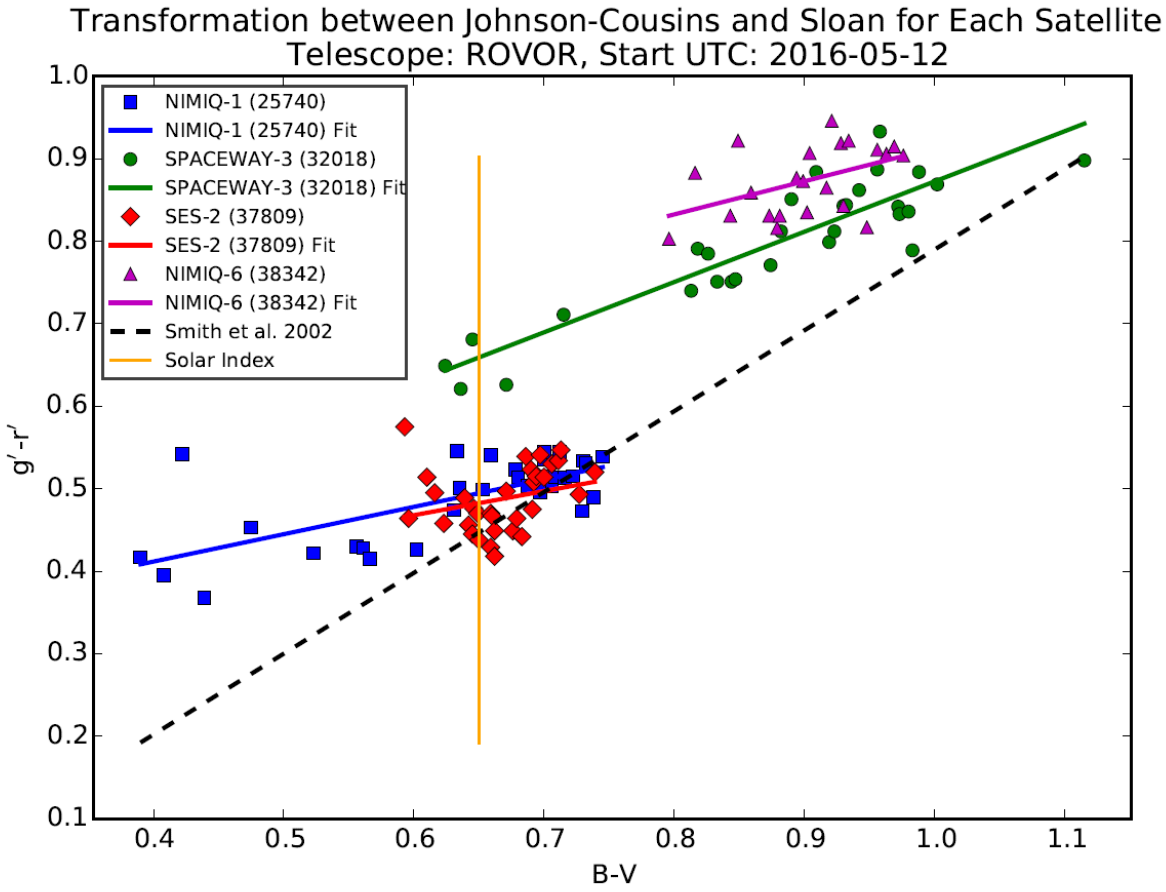

Fig. 27. $g' - r'$ as a function of $B - V$ transformations of each satellite with the observed data and fit, the astronomical transformation of [20], and the solar color index.

Fig. 28 shows the total satellite transformation. The observed data is a great fit to the linear transformation. The satellite transformation lies above the astronomical transformation with a slightly different slope. The RMS is large at 0.08 mag. The satellite transformation is within three sigma of the astronomical transformation. Note how the few data points at the blue end are above the satellite transformation. This pulls the linear fit upward so that the majority of satellite data just red of this are now below the satellite transformation. The difference between the observed data and the satellite transformation contains significant scatter, partially due to this, with differences as large as 0.3 mag at the bluer color indices and scatter for much of the data ranging from zero to around 0.1 mag. The differences to the astronomical transformation are more severe for the data in general, with deviations as large as around 0.3 mag.

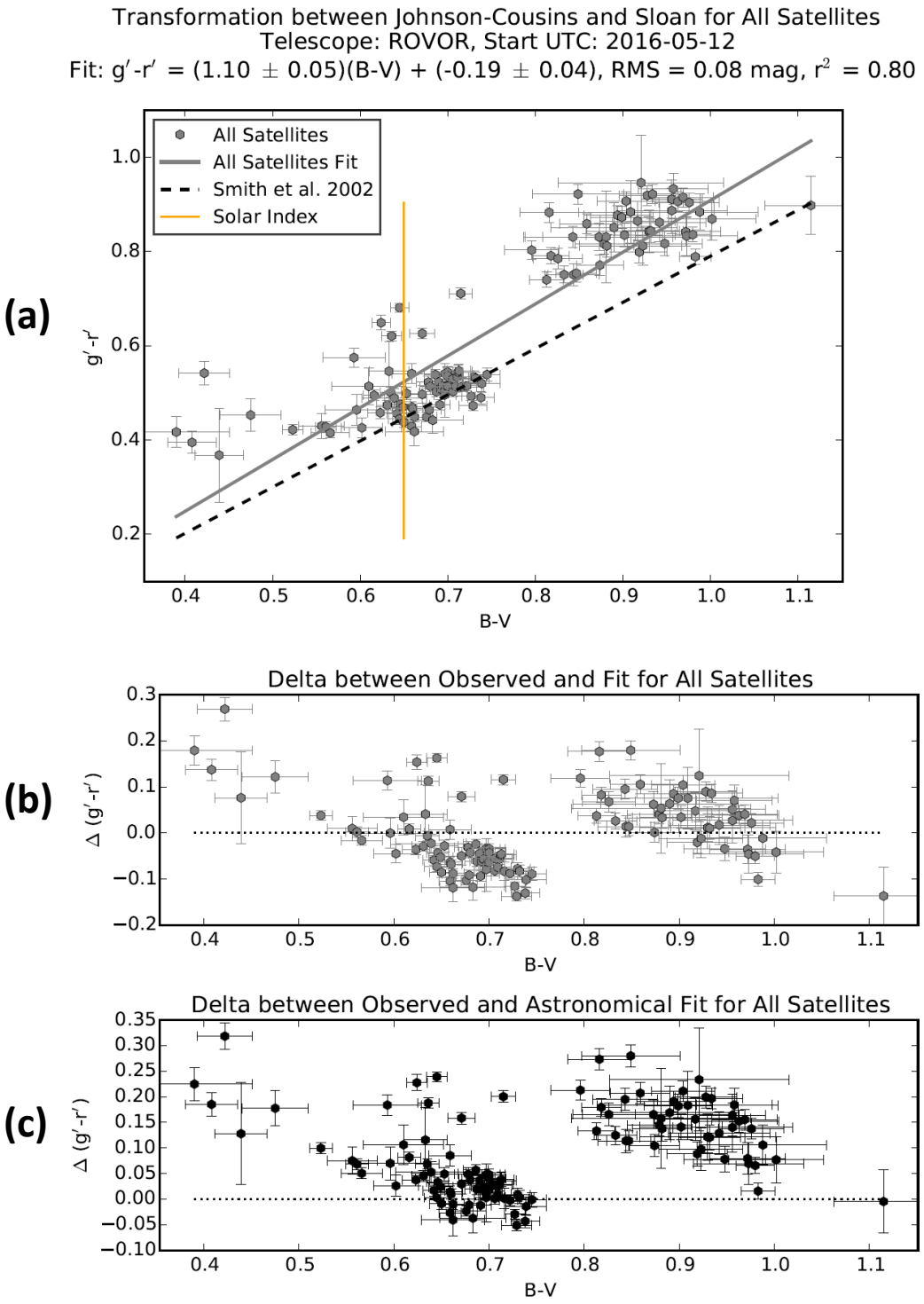

Fig. 28. (a) $g' - r'$ as a function of $B - V$ transformation for all of the satellites with our observed data and fit, the astronomical transformation of [20], and the solar color index, (b) the difference between the observed data and our fit, and (c) the difference between the observed data and the astronomical transformation.

Tab. 8 shows a summary of the $g' - r'$ as a function of $B - V$ relation. This relation provides a valid fit for the total satellite transformation but has a large RMS, and deviates by up to three sigma from the astronomical transformation. The valid individual satellite transformations are distinctly different from the astronomical transformation. Therefore, there is an inconsistency between individual satellite transformations and the total satellite transformation. Recall, that the astronomical transformation relation of [29] differs for the $g' - r'$ relation and is a function of $B - V$ and $V - R$. Investigating a transformation relation with two Johnson-Cousins colors may improve the results for this relation.

Tab. 8. Summary of the $g' - r'$ as a function of $B - V$ relation.

Satellite	r^2	RMS (mag)	σ from Astronomical Transformation
NIMIQ-1 (25740)	0.49 (good fit)	0.04	> 3 (distinct)
SPACEWAY-3 (32018)	0.82 (great fit)	0.03	> 3 (distinct)
SES-2 (37809)	0.07 (poor fit)	…	…
NIMIQ-6 (38342)	0.21 (poor fit)	…	…
All	0.80 (great fit)	0.08	< 3

3.5 $r' - i'$ as a Function of $R - I$ Relation

Fig. 29 shows the transformation for NIMIQ-1 (25740). The observed data is a poor fit to the linear transformation. There are two outliers at the red end of the $R - I$ color index that may be partly responsible for the poor fit, as the remainder of the data appears to form a linear trend.

Fig. 30 shows the transformation for SPACEWAY-3 (32018). The observed data is a good fit to the linear transformation, intersecting the astronomical transformation. The RMS scatter is moderate. Our transformation is comparable within three sigma of the astronomical transformation. The difference between the observed data and the satellite transformations is mostly less than 0.05 mag but with some differences around 0.1 mag. The difference for the astronomical transformation is comparable to the satellite transformation.

Fig. 31 shows the transformation for SES-2 (37809). The observed data is a good fit to the linear transformation, intersecting the astronomical transformation. The RMS scatter is small. Our transformation is comparable within two sigma of the astronomical transformation. The difference between the observed data and the satellite transformation is mostly within 0.05 mag but with one data point 0.1 mag from the fit. The differences with the astronomical transformation is similar to the satellite transformation.

Fig. 32 shows the transformation for NIMIQ-6 (38342). The observed data is a poor fit to the linear transformation. The one data point at the redder color indices of $R - I$ has large error bars. This outlier along with the one data point to the upper left of it may be responsible for the poor fit because the remainder of the data lies along the astronomical transformation in what appears to form a linear trend.

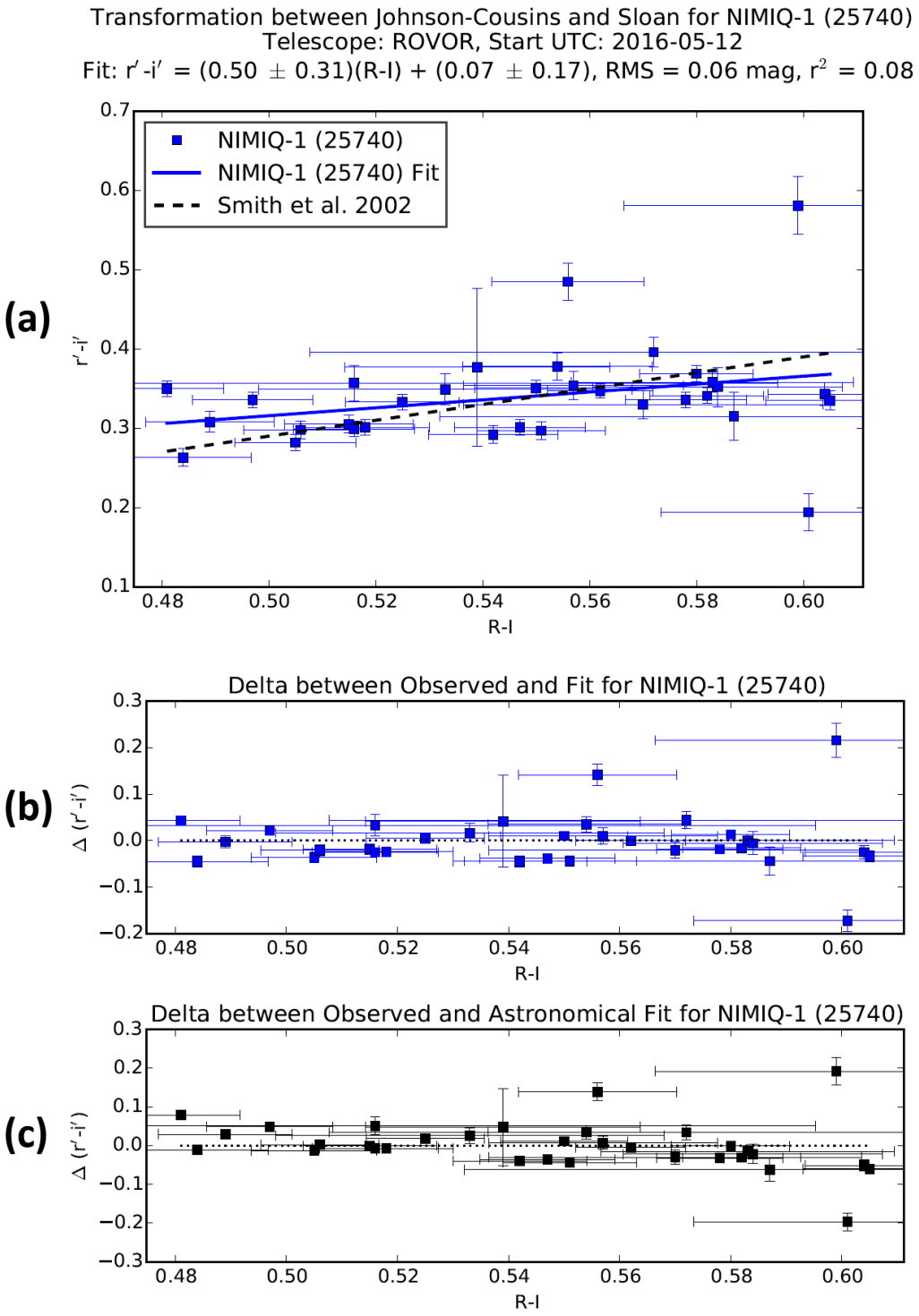

Fig. 29. (a) $r' - i'$ as a function of $R - I$ transformations for NIMIQ-1 (25740) with our observed data and fit, the astronomical transformation of [20], and the solar color index, (b) the difference between the observed data and our fit, and (c) the difference between the observed data and the astronomical transformation.

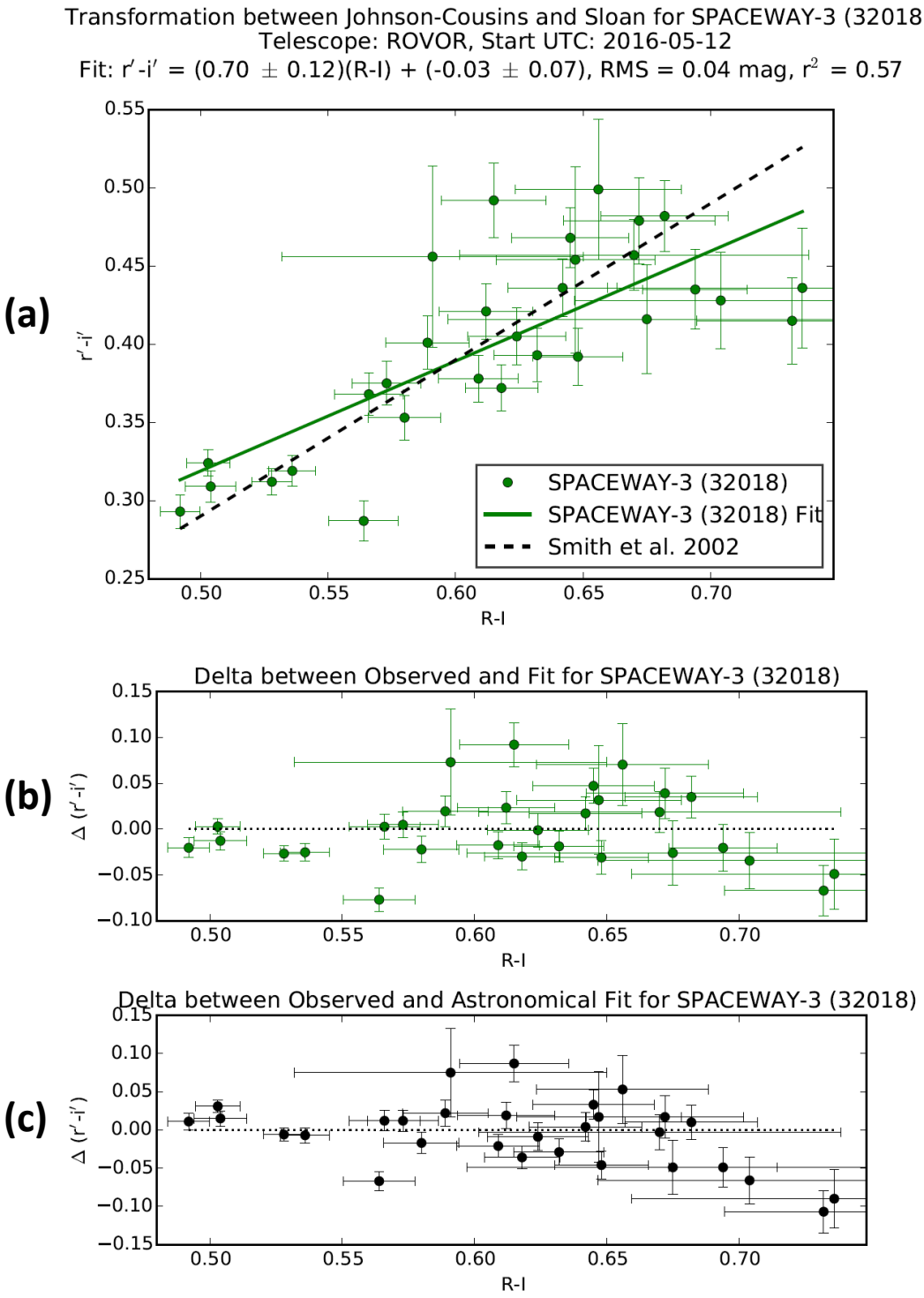

Fig. 30. (a) $r' - i'$ as a function of $R - I$ transformations for SPACEWAY-3 (32018) with our observed data and fit, the astronomical transformation of [20], and the solar color index, (b) the difference between the observed data and our fit, and (c) the difference between the observed data and the astronomical transformation.

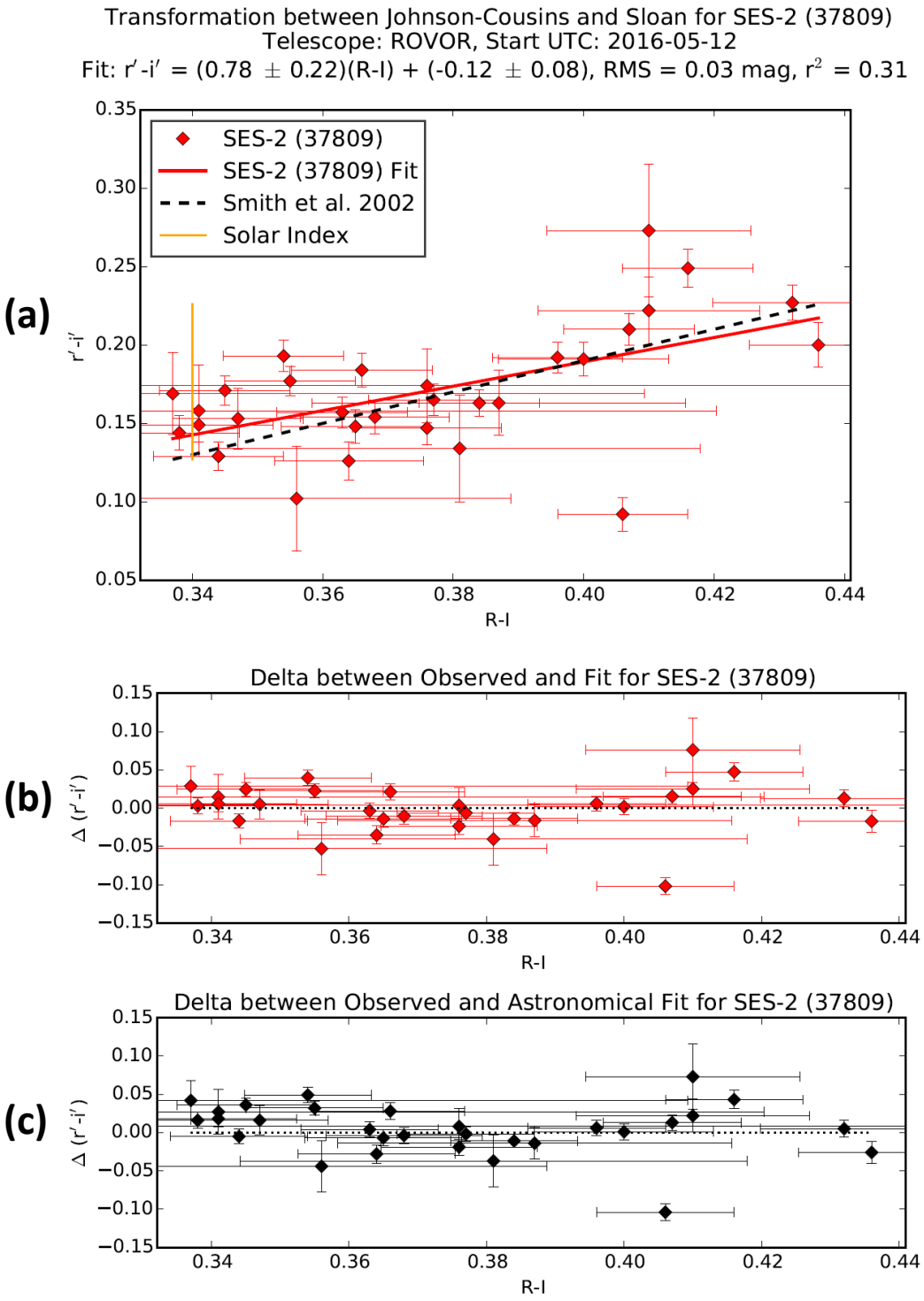

Fig. 31. (a) $r' - i'$ as a function of $R - I$ transformations for SES-2 (37809) with our observed data and fit, the astronomical transformation of [20], and the solar color index, (b) the difference between the observed data and our fit, and (c) the difference between the observed data and the astronomical transformation.

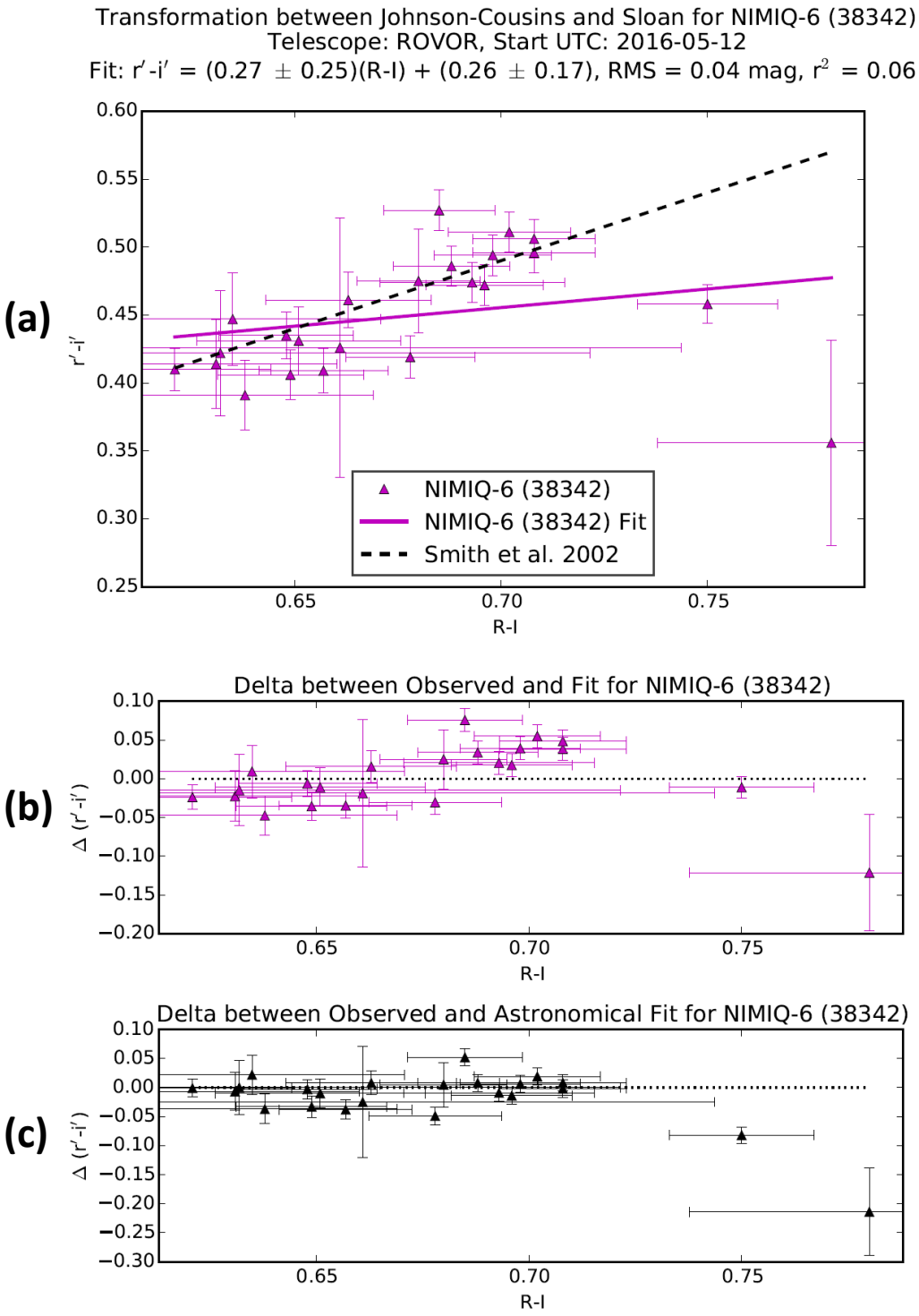

Fig. 32. (a) $r' - i'$ as a function of $R - I$ transformations for NIMIQ-6 (38342) with our observed data and fit, the astronomical transformation of [20], and the solar color index, (b) the difference between the observed data and our fit, and (c) the difference between the observed data and the astronomical transformation.

Fig. 33 shows the transformations for each of the satellites plotted together. All of the observed data appears to largely lie along the astronomical transformation, except for a few extreme outliers of NIMIQ-1 (25740) and NIMIQ-6 (38342). The transformation for each satellite intersects the astronomical transformation but with different slopes from each other. Again the color index range spanned by all of the satellite data is significantly larger than that of the individual satellites. The valid individual transformations appear to be similar visually in their own region of color index space; they have similar slopes and pass through the astronomical transformation.

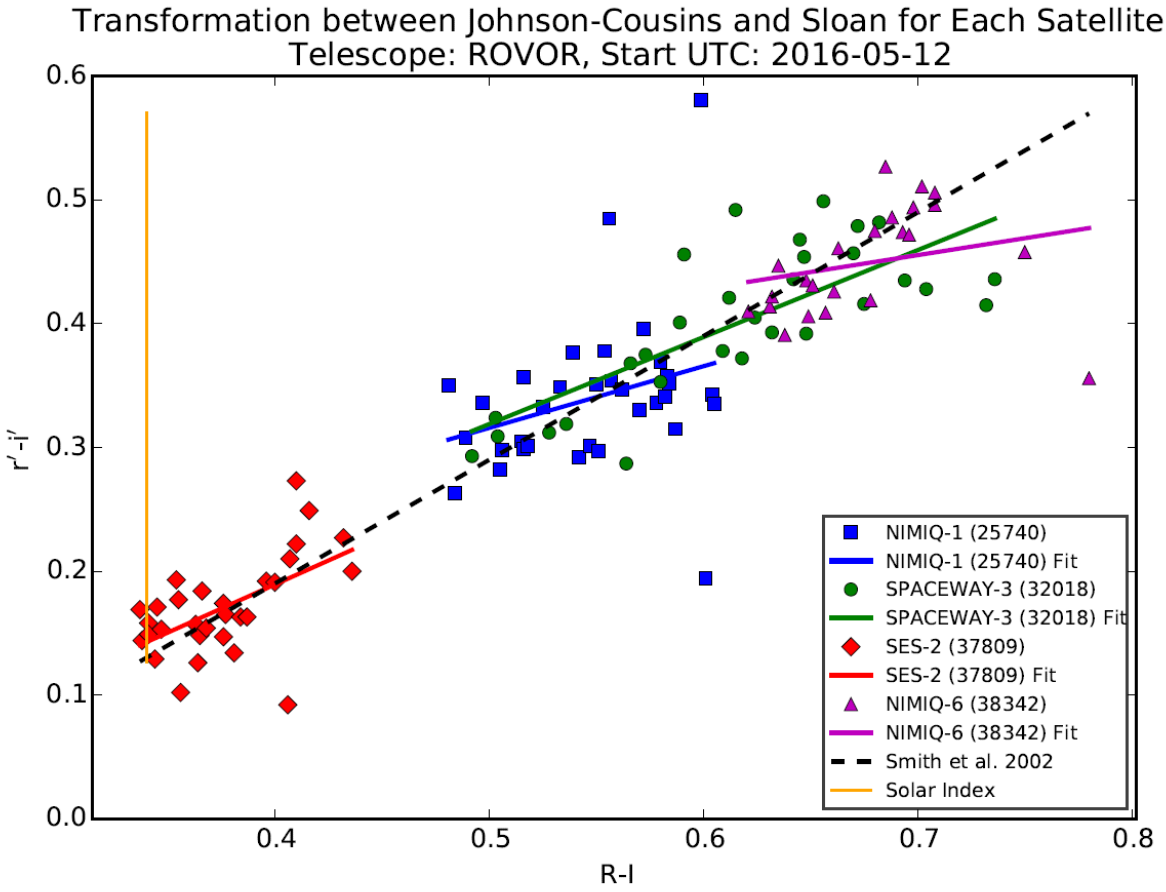

Fig. 33. $r' - i'$ as a function of $R - I$ transformations of each satellite with the observed data and fit, the astronomical transformation of [20], and the solar color index.

Fig. 34 shows the total satellite transformation. The observed data is a great fit to the linear transformation. The satellite transformation is similar to the astronomical transformation, but still intersecting it. The RMS is large at 0.05 mag. The total satellite transformation is within three sigma of the astronomical transformation. The difference between the observed data and the satellite transformation is large, with most of the data within 0.1 mag, but some data outliers are as far as 0.2 mag from the fit. The difference with the astronomical transformation is similar to the satellite transformation.

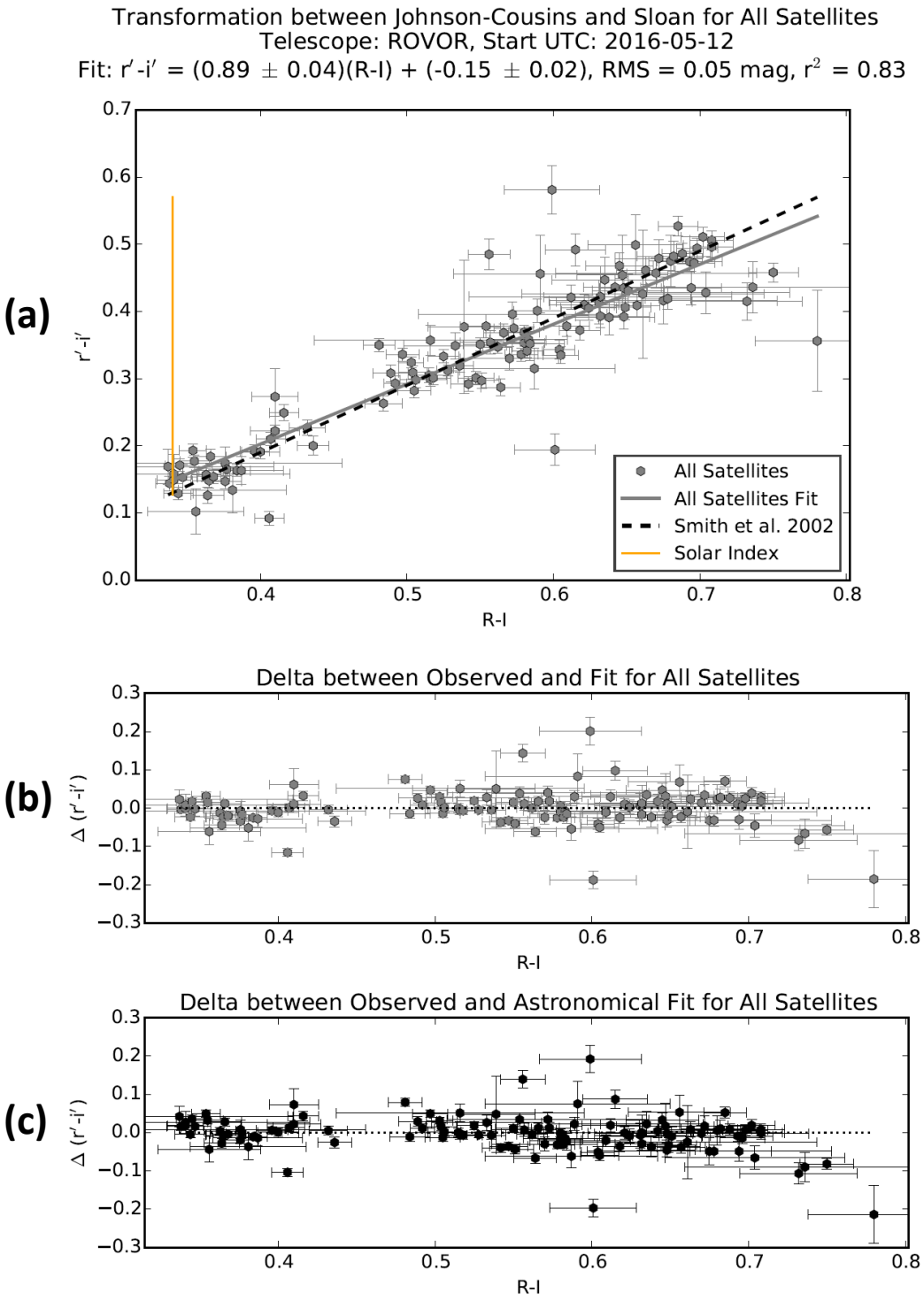

Fig. 34. (a) $r' - i'$ as a function of $R - I$ transformation for all of the satellites with our observed data and fit, the astronomical transformation of [20], and the solar color index, (b) the difference between the observed data and our fit, and (c) the difference between the observed data and the astronomical transformation.

Tab. 9 shows a summary of the $r' - i'$ as a function of $R - I$ relation. This relation provides a valid fit for the total satellite transformation, but has a large RMS and deviates by up to three sigma from the astronomical transformation. The valid individual satellite transformations are comparable to the astronomical transformation, meaning that all the valid transformations are consistent with each other.

Tab. 9. Summary of the $r' - i'$ as a function of $R - I$ relation.

Satellite	r^2	RMS (mag)	σ from Astronomical Transformation
NIMIQ-1 (25740)	0.08 (poor fit)	…	…
SPACEWAY-3 (32018)	0.57 (good fit)	0.04	< 3
SES-2 (37809)	0.31 (good fit)	0.03	< 2
NIMIQ-6 (38342)	0.06 (poor fit)	…	…
All	0.83 (great fit)	0.05	< 3

3.6 $r' - z'$ as a Function of $R - I$ Relation

Fig. 35 shows the transformation for NIMIQ-1 (25740). The observed data is a poor fit to the linear transformation. Fig. 36 shows the transformation for SPACEWAY-3 (32018). The observed data is a great fit to the linear transformation (r^2 is large), although the RMS is large. The satellite transformation has a slightly different slope but is shifted lower than the astronomical transformation so that they do not intersect. Our transformation is within one sigma of the astronomical transformation. The difference between the observed data and the satellite transformation is large, with most values within about 0.05 mag and a handful of values up to almost 0.15 mag away from the fit. The difference for the astronomical transformation has most of the data within about 0.1 mag with a few data points slightly farther from the fit.

Fig. 37 shows the transformation for SES-2 (37809). The observed data is a poor fit to the linear transformation. Fig. 38 shows the transformation for NIMIQ-6 (38342). The observed data is a good fit to the linear transformation with small RMS error. The satellite transformation does not intersect the astronomical transformation; it is shifted lower with a different slope. The satellite transformation is distinct (outside of three sigma) from the astronomical transformation. Note the two data points at the red color end of $R - I$ pull down the satellite linear fit causing it to be different from the astronomical transformation. Although one data point has large error bars the other does not, so it appears that this effect is real and not due to spurious data. The difference between the observed data and the satellite transformation is large, with most of the data within about 0.05 mag. The difference for the astronomical transformation is significantly worse, with most of the data within about 0.1 mag and a few data points (the outliers) as far as 0.2 mag away from the fit.

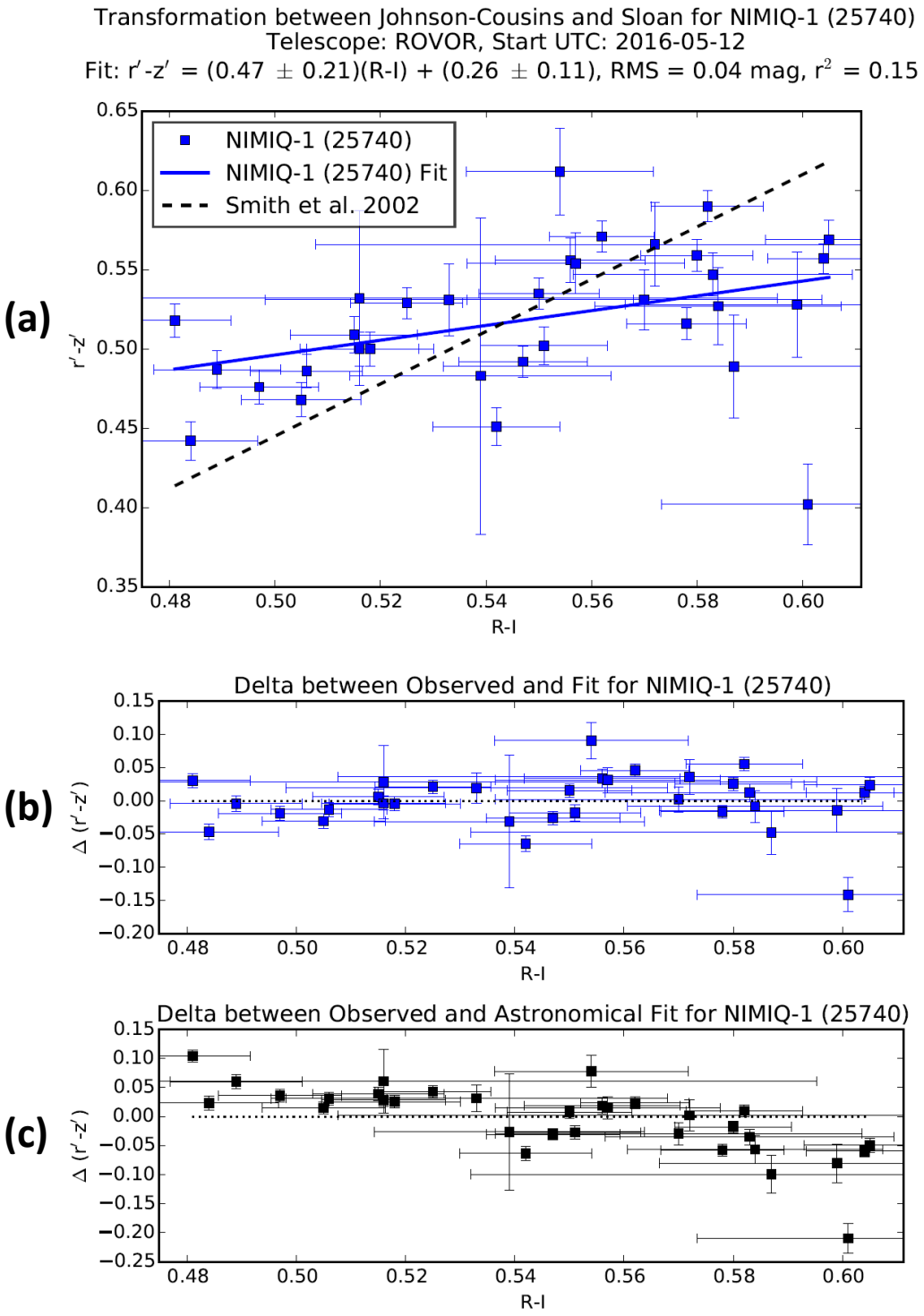

Fig. 35. (a) $r' - z'$ as a function of $R - I$ transformations for NIMIQ-1 (25740) with our observed data and fit, the astronomical transformation of [20], and the solar color index, (b) the difference between the observed data and our fit, and (c) the difference between the observed data and the astronomical transformation.

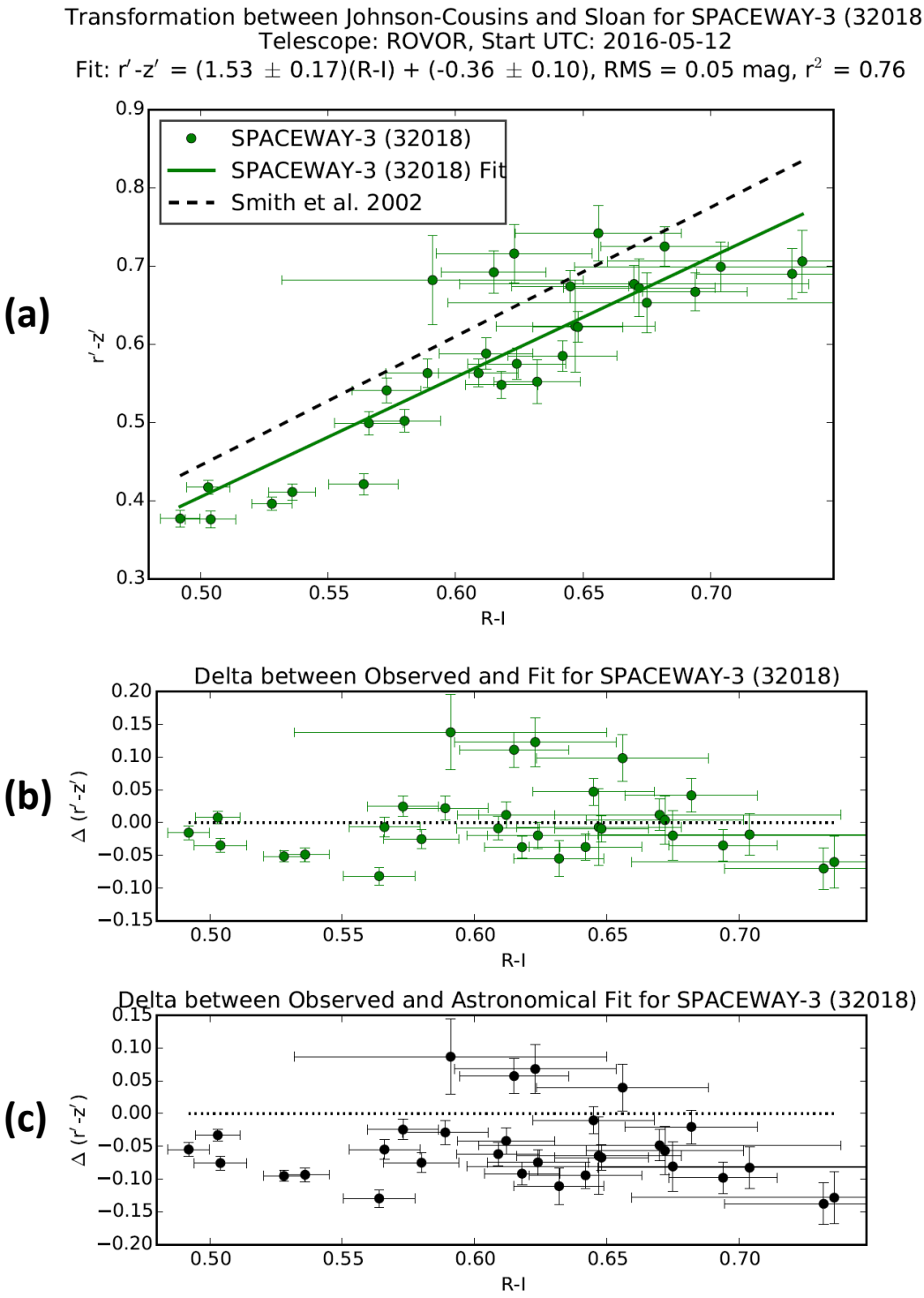

Fig. 36. (a) $r' - z'$ as a function of $R - I$ transformations for SPACEWAY-3 (32018) with our observed data and fit, the astronomical transformation of [20], and the solar color index, (b) the difference between the observed data and our fit, and (c) the difference between the observed data and the astronomical transformation.

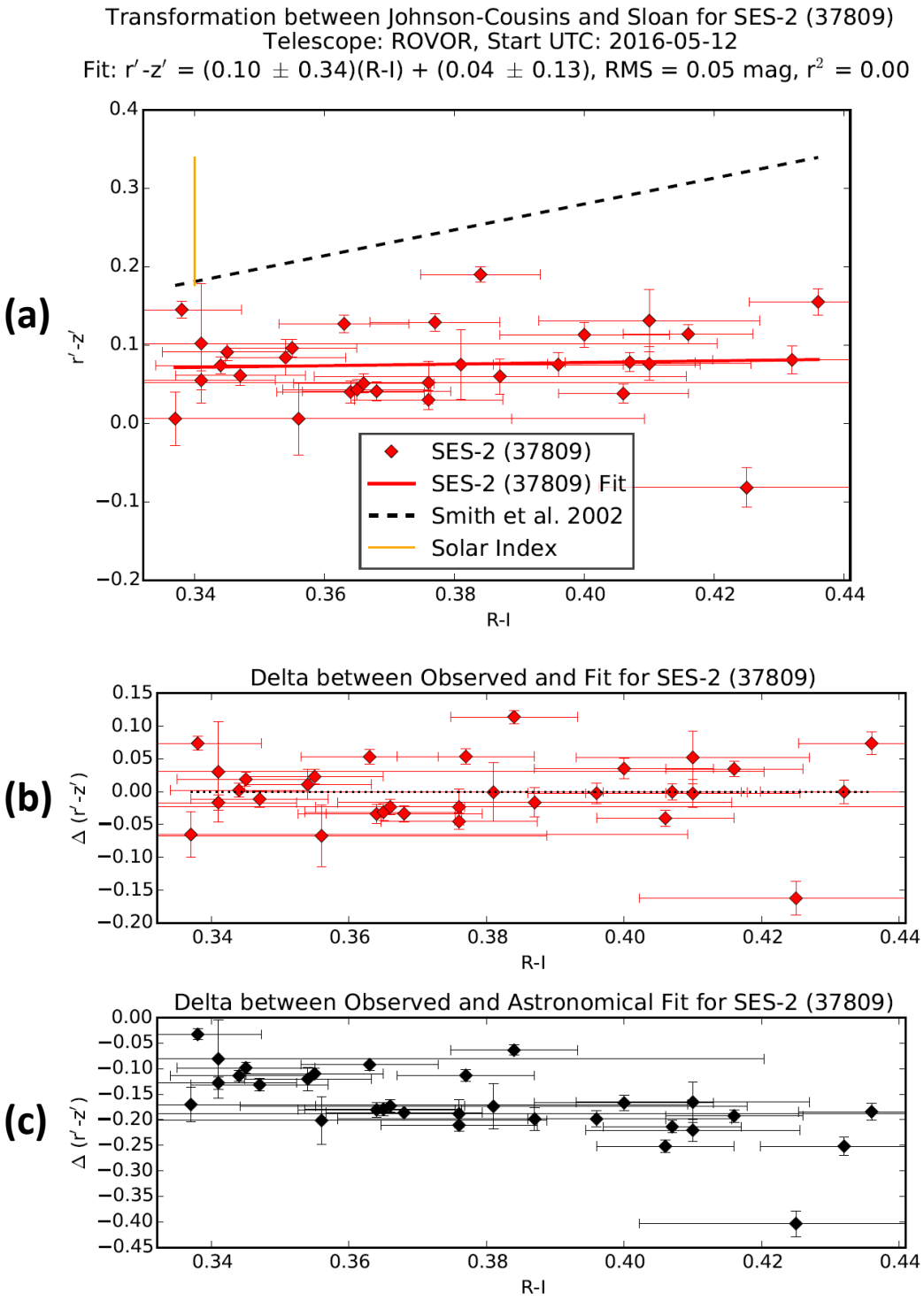

Fig. 37. (a) $r' - z'$ as a function of $R - I$ transformations for SES-2 (37809) with our observed data and fit, the astronomical transformation of [20], and the solar color index, (b) the difference between the observed data and our fit, and (c) the difference between the observed data and the astronomical transformation.

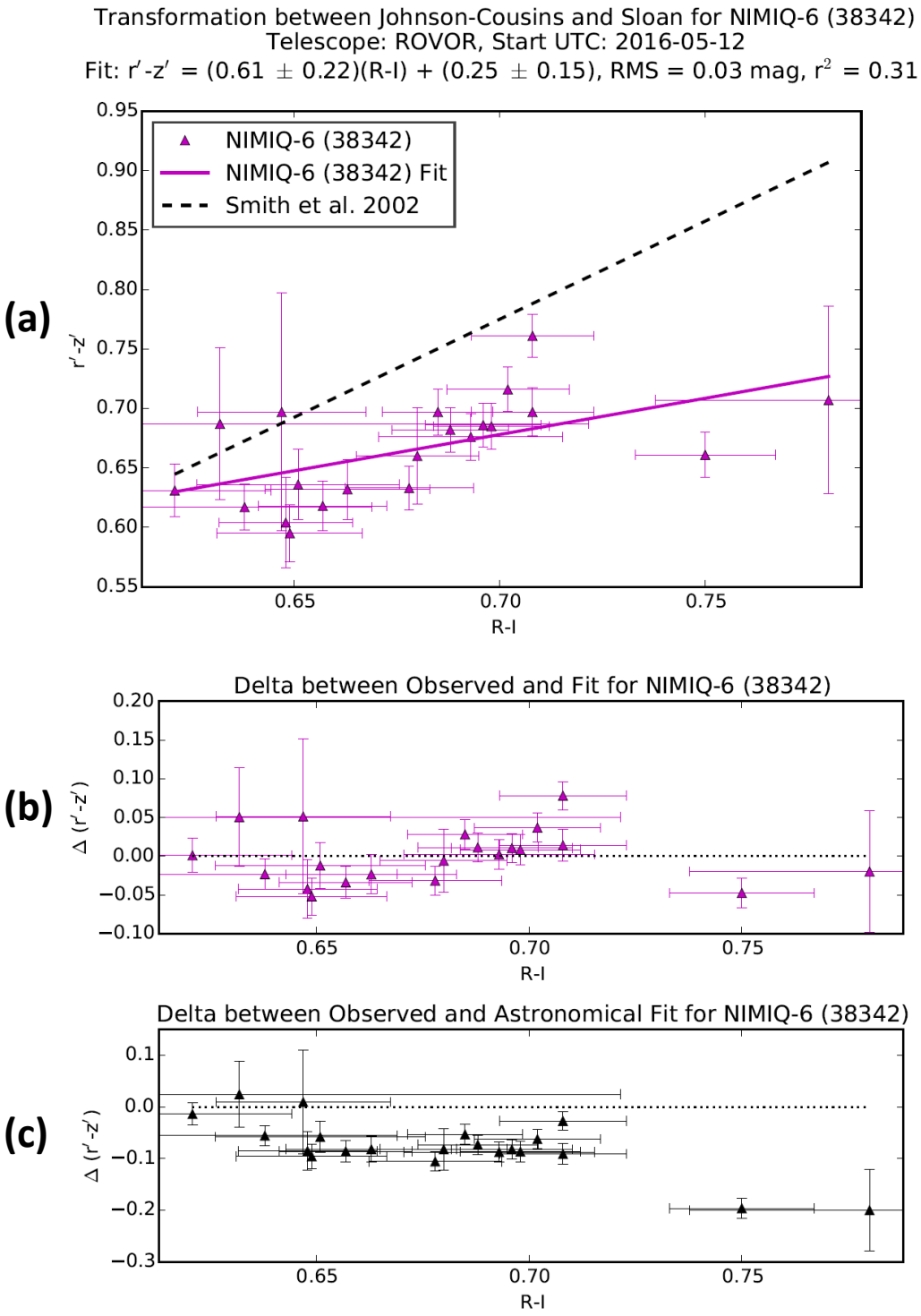

Fig. 38. (a) $r' - z'$ as a function of $R - I$ transformations for NIMIQ-6 (38342) with our observed data and fit, the astronomical transformation of [20], and the solar color index, (b) the difference between the observed data and our fit, and (c) the difference between the observed data and the astronomical transformation.

Fig. 39 shows the transformations for each of the satellites. All of the observed data lies mostly below the astronomical transformation, with the valid satellite transformations not intersecting the astronomical transformation, but below it. Again, the span of all of the satellite data in color index space is significantly larger than that of the individual satellites. The valid individual satellite transformations are not similar visually, with different slopes and overlapping in color-color space. If not for two data points that are outliers for NIMIQ-6 (38342), one with small error bars and one with large error bars, the two transformations would look quite similar.

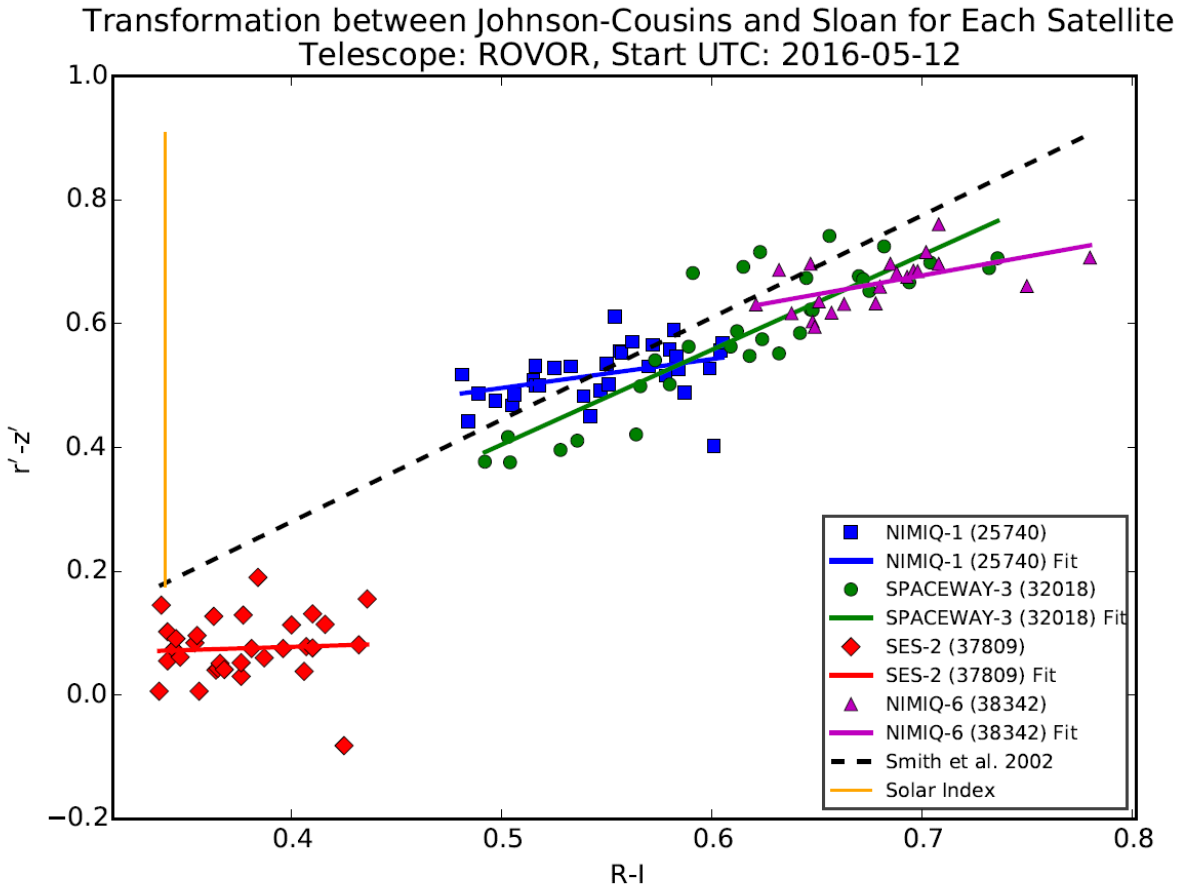

Fig. 39. $r' - z'$ as a function of $R - I$ transformations of each satellite with the observed data and fit, the astronomical transformation of [20], and the solar color index.

Fig. 40 shows the total satellite transformation. The observed data is a great fit to the linear transformation. The satellite transformation lies below the astronomical transformation with a slightly different slope, which would intersect the astronomical linear fit line at the extreme red end of R-I. However, the RMS is large at 0.08 mag. Our transformation is distinct (outside of three sigma) from the astronomical transformation. The difference between the observed data and the satellite transformation is extreme, with values up to 0.2 mag, and an outlier at 0.3 mag. While the difference for the astronomical transformation is slightly larger, with values slightly above 0.2 mag and an outlier at 0.4 mag.

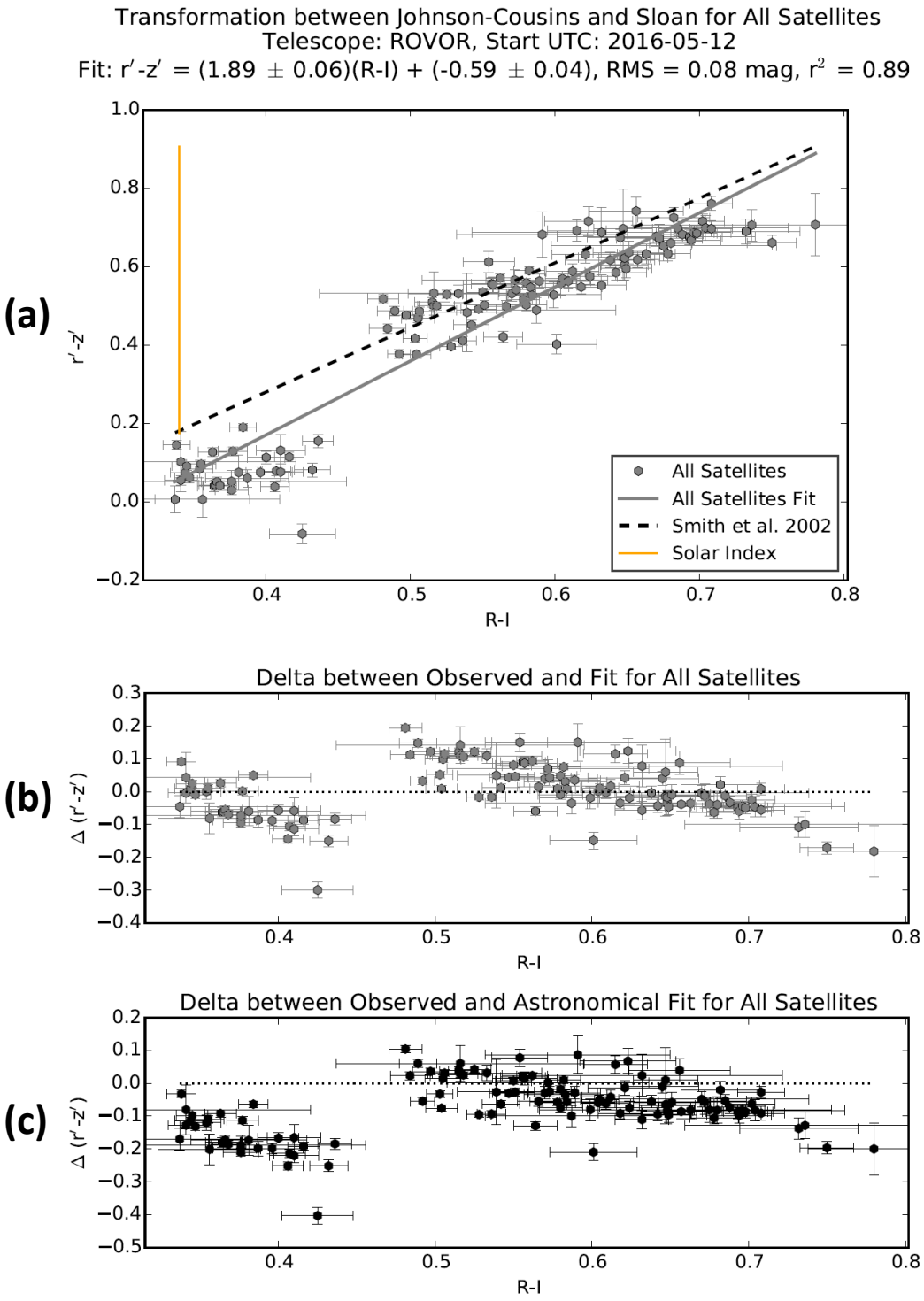

Fig. 40. (a) $r' - z'$ as a function of $R - I$ transformation for all of the satellites with our observed data and fit, the astronomical transformation of [20], and the solar color index, (b) the difference between the observed data and our fit, and (c) the difference between the observed data and the astronomical transformation.

Tab. 10 shows a summary of the $r' - z'$ as a function of $R - I$ relation. This relation provides a valid fit for the total satellite transformation, but has a large RMS and is distinct from the astronomical transformation. While for the valid individual satellite transformations, one is comparable and one is distinct from the astronomical transformation. There is discrepancy between the individual satellite transformations (one is the same as the astronomical and one is different) and the satellite transformation using all the satellites. The latter is also significantly different from the astronomical transformation.

Tab. 10. Summary of the $r' - z'$ as a function of $R - I$ relation.

Satellite	r^2	RMS (mag)	σ from Astronomical Transformation
NIMIQ-1 (25740)	0.15 (poor fit)	…	…
SPACEWAY-3 (32018)	0.76 (great fit)	0.05	< 1
SES-2 (37809)	0.00 (poor fit)	…	…
NIMIQ-6 (38342)	0.31 (good fit)	0.03	> 3 (distinct)
All	0.89 (great fit)	0.08	> 3 (distinct)

4. CONCLUSIONS

This analysis investigated the transformation between Johnson-Cousins and Sloan photometric systems for satellites. For the four filters in each photometric system, there are six transformation relationships. The transformation relationships we derived provide mixed results with the best transformation relationship being that of $r' - V$ as a function of $V - R$. The observed data fit the total satellite transformation with low RMS error and is exactly the same as the astronomical transformation for this relation. On the other hand, the $r' - z'$ as a function of $R - I$ relation provides a great fit for the total satellite transformation but has a large RMS error and is significantly different from the astronomical transformation. Additionally, for this relationship, there is inconsistency between the individual satellite transformations and the total satellite transformation. The transformation relationships for the other filters yielded similar discrepant results. With only one reliable transformation relation, there is minimal utility.

Data available for this analysis were on four satellites. To provide compelling conclusions that are broader, a much larger sample would have been preferable. Astronomical transformations utilize a broad range of color indices by including diverse spectral types with largely static SEDs (color indices). The satellite transformations investigated here are different in that we have only sampled a small fraction of the satellite population where the range of color index for each satellite varies throughout the night, i.e., their SEDs change slightly throughout the night. Our conclusions are constrained by the small sample size, although the sample represents the different types (and colors) of three-axis stabilized geosynchronous satellites well. In addition, the results presented here use only non-glint season data. An analysis of satellites during glint season would contain more specular reflections. Glinting satellites have previously shown more extreme color indices, and we expect larger spectral changes during glint season that do not occur at other times.

Given the evolution of satellite SEDs with season, where during equinoctial glints the satellite SED can change dynamically, we do not expect additional analysis on a broader data set of satellites and seasonal sampling to improve the transformation results. As a matter of fact, this variability would only exacerbate the fits that derive the transformations. Because satellite SEDs are in general dynamic in time and dependent on illumination and observing geometries, our concern that the dynamic nature of satellite SEDs could cause photometry error in the transformed photometry was justified. The mixed results are due to the satellite SED variability.

Furthermore, transformations are only valid over the range of color indices from which they were derived and therefore should not be extrapolated outside of this range. Based on this work, we *do not* recommend transforming historical satellite photometry observed in Johnson-Cousins to the Sloan filters for the purpose of comparing the historical

photometry to photometry collected in Sloan. Finally, this paper's conclusions on the transformations can be generalized to deriving transformations between any two photometric systems using satellite photometry. Since the transformations are inherently dependent on the SED of the satellite and the behavior of satellite SED throughout the night is such that transformations between Johnson-Cousins and Sloan are poor, transformations between any other two photometric systems will not yield consistent results either.

5. ACKNOWLEDGEMENTS

We acknowledged the support of the Spacecraft Object Tracking and Characterization program and its program manager Ms. Virginia Wright.

6. REFERENCES

[1] H. L. Johnson and W. W. Morgan, "Fundamental Stellar Photometry for Standards of Spectral Type on the Revised System of the Yerkes Spectral Atlas," *The Astrophysical Journal,* vol. 117, pp. 313-352, 1953.

[2] H. L. Johnson, R. I. Mitchell, B. Iriarte and W. Z. Wisniewski, "UBVRIJKL Photometry of the Bright Stars," *Communications of the Lunar and Planetary Laboratory,* vol. 4, p. 99, 1966.

[3] M. S. Bessell, "Standard Photometric Systems," *Annual Review of Astronomy & Astrophysics,* vol. 43, pp. 293-336, 2005.

[4] G. E. Kron, H. S. White and S. C. B. Gascoigne, "Red and Infrared Magnitudes for 138 Stars Observed as Photometric Standards," *The Astrophysical Journal,* vol. 118, pp. 502-510, 1953.

[5] A. W. J. Cousins, "VRI Standards in the E Regions," *Memoirs of the Royal Astronomical Society,* vol. 81, pp. 25-36, 1976.

[6] A. U. Landolt, "UBVRI Photometric Standard Stars Around the Celestial Equator," *The Astronomical Journal,* vol. 88, pp. 439-460, 1983.

[7] A. U. Landolt, "UBV Photoelectric Sequences in the Celestial Equatorial Selected Areas," *The Astronomical Journal,* vol. 78, pp. 959-1021, 1973.

[8] B. D. Warner, A Practical Guide to Lightcurve Photometry and Analysis, New York: Springer, 2006.

[9] A. U. Landolt, "UBVRI Photometric Standard Stars in the Magnitude Range 11.5 < V < 16.0 Around the Celestial Equator," *The Astronomical Journal,* vol. 104, pp. 340-491, 1992.

[10] A. U. Landolt, "UBVRI Photometric Standard Stars Around the Celestial Equator: Updates and Additions," *The Astronomical Journal,* vol. 137, pp. 4186-4269, 2009.

[11] A. U. Landolt, "UBVRI Photometric Standard Stars Around the Sky at +50 deg Declination," *The Astronomical Journal,* vol. 146, p. 131, 2013.

[12] T. E. Payne, S. A. Gregory, D. J. Sanchez, L. G. Finkner, D. M. Payne, L. Kann, C. K. Davis and D. Werling, "Space Object Identification of Geosynchronous Satellites," in *AMOS Technical Conference*, 1999.

[13] T. E. Payne, S. A. Gregory, J. Tombasco, K. Luu and L. Durr, "Satellite Monitoring, Change Detection, and Characterization Using Non-Resolved Electro-Optical Data from a Small Aperture Telescope," in *AMOS*, 2007.

[14] M. Fukugita, T. Ichikawa, J. E. Gunn, M. Doi, K. Shimasaku and D. P. Schneider, "The Sloan Digital Sky Survey Photometric System," *The Astronomical Journal* , vol. 111, pp. 1748-1756, 1996.

[15] D. G. York, J. Adelman, J. E. Anderson Jr., S. F. Anderson, J. Annis, N. A. Bahcall, J. A. Bakken, R. Barkhouser, S. Bastian, E. Berman, W. N. Boroski, S. Bracker, C. Briegel and J. W. Briggs, "The Sloan Digital Sky Survey: Technical Summary," *The Astronomical Journal,* vol. 120, pp. 1579-1587, 2000.

[16] K. N. Abazajian, J. K. Adelman-McCarthy, M. A. Agueros, S. S. Allam, C. A. Prieto, D. An, K. S. J. Anderson, S. F. Anderson, J. Annis, N. A. Bahcall, C. A. L. Bailer-Jones and J. C. Barentine, "The Seventh Data Release of the Sloan Digital Sky Survey," *The Astrophysical Journal Supplement Series,* vol. 182, pp. 543-558, 2009.

[17] J. L. Tonry, C. W. Stubbs, K. R. Lykke, P. Doherty, I. S. Shivvers, W. S. Burgett, K. C. Chambers, K. W. Hodapp, N. Kaiser, R. P. Kudritzki, E. A. Magnier, J. S. Morgan, P. A. Price and R. J. Wainscoat, "The Pan-STARRS1 Photometric System," *The Astrophysical Journal,* vol. 750, p. 99, 2012.

[18] E. A. Magnier, E. Schlafly, D. Finkbeiner, M. Juric, J. L. Tonry, W. S. Burgett, K. C. Chambers, H. A. Flewelling, N. Kaiser, R. P. Kudritzki, J. S. Morgan, P. A. Price, W. E. Sweeney and C. W. Stubbs, "The Pan-STARRS 1 Photometric Reference Ladder, Release 12.01," *The Astrophysical Journal Supplement Series,* vol. 205, p. 20, 2013.

[19] M. Fukugita, T. Ichikawa, J. E. Gunn, M. Doi, K. Shimasaku and D. P. Schneider, "The Sloan Digital Sky Survey Photometric System," *The Astronomical Journal* , vol. 111, pp. 1748-1756, 1996.

[20] J. A. Smith, D. L. Tucker, S. Kent, M. W. Richmond, M. Fukugita, T. Ichikawa, S.-I. Ichikawa, A. M. Jorgensen, A. Uomoto, J. E. Gunn, M. Hamabe, M. Watanabe, A. Tolea and A. Henden, "The u'g'r'i'z' Standard-Star System," *The Astronomical Journal,* vol. 123, pp. 2121-2144, 2002.

[21] J. E. Gunn and L. L. Stryker, "Stellar Spectrophotometric Atlas, 3130 < Lambda < 10800 Angstroms," *The Astrophysical Journal Supplement Series,* pp. 121-153, 1983.

[22] J. B. Oke, "Faint Spectrophotometric Standard Stars," *The Astronomical Journal,* p. 1621, 1990.

[23] S. Jester, D. P. Schneider, G. T. Richards, R. F. Green, M. Schmidt, P. B. Hall, M. A. Strauss, D. E. Vanden Berk, C. Stoughton, J. E. Gunn, J. Brinkmann, S. M. Kent and J. A. Smith, "The Sloan Digital Sky Survey View of the Palomar-Green Bright Quasar Survey," *The Astronomical Journal,* vol. 130, pp. 873-895, 2005.

[24] C. Stoughton, R. H. Lupton, M. Bernardi, M. R. Blanton, S. Burles, F. J. Castander, A. J. Connolly, D. J. Eisenstein, J. A. Frieman, G. S. Hennessy, R. B. Hindsley, Z. Ivezic and S. Kent, "Sloan Digital Sky Survey: Early Data Release," *The Astronomical Journal,* pp. 485-548, 2002.

[25] S. Karaali, S. Bilir and S. Tuncel, "New Colour Transformations for the Sloan Photometry, and Revised Metallicity Calibration and Equations for Photometric Parallax Estimation," *Publications of the Astronomical Society of Australia,* pp. 24-28, 2005.

[26] K. Jordi, E. K. Grebel and K. Ammon, "Empirical Color Transformations between SDSS Photometry and other Photometric Systems," *Astronomy & Astrophysics,* vol. 460, pp. 339-347, 2006.

[27] P. B. Stetson, "Homogeneous Photometry for Star Clusters and Resolved Galaxies. II. Photometric Standard Stars," *Publications of the Astronomical Society of the Pacific,* vol. 112, pp. 925-931, 2000.

[28] P. J. Castro, T. E. Payne, A. M. Battle, Z. W. Cole, J. W. Moody, S. A. Gregory and P. D. Dao, "Standardized Photometric Calibrations for Panchromatic SSA Sensors," in *2016 AMOS Conference Proceedings*, Wailea, 2016.

[29] C. T. Rodgers, R. Canterna, J. A. Smith, M. J. Pierce and D. L. Tucker, "Improved u'g'r'i'z' to UBVRcIc Transformation Equations for Main-Sequence Stars," *The Astronomical Journal,* vol. 132, pp. 989-993, 2006.

[30] J. R. A. Davenport, A. A. West, C. K. Matthiesen, M. Schmieding and A. Kobelski, "Sloan/Johnson-Cousins/2MASS Color Transformations for Cool Stars," *Publications of the Astronomical Society of the Pacific,* vol. 118, pp. 1679-1684, 2006.

[31] T. E. Payne, P. J. Castro, J. W. Moody, E. A. Beecher, M. D. Fisher and R. I. Acosta, "A Discrimination Analysis of Sloan and Johnson Photometric Systems for Non-Resolved Object Characterization," in *AMOS Conference Proceedings*, 2016.

[32] J. W. Moody, B. Boizelle, K. Bates, B. Little, T. McCombs, J. Nelson, C. Pace, R. L. I. Pearson, J. Harrison, P. J. Brown and J. Barnes, "Remote Observatory for Variable Object Research (ROVOR)," *Publications of the Astronomical Society of the Pacific,* vol. 124, pp. 956-962, 2012.

[33] F. E. Nicodemus, J. C. Richmond, J. J. Hsia, I. W. Ginsberg and T. Limperis, "Geometrical Considerations and Nomenclature for Reflectance," Department of Commerce, National Bureau of Standards, 1977.

[34] R. L. Cook and K. E. Torrance, "A Reflectance Model for Computer Graphics," *ACM Transactions on Graphics*, pp. 7-24, 1982.

[35] D. E. Weisz and F. K. Chun, "Comparison of Geosynchronous Satellites Spectral Signatures During Glint Season," in *AMOS Technical Conference*, 2017.

[36] J. V. Lambert, "Measurement of the Visible Reflectance Spectra of Orbiting Satellites," Air Force Institute of Technology, Dayton, OH, 1971.

[37] F. J. Vrba, M. E. DiVittorio, R. B. Hindsley, H. R. Schmitt, J. T. Armstrong, P. D. Shankland, D. J. Hutter and J. A. Benson, "A Survey of Geosynchronous Satellite Glints," in *AMOS Conference Proceedings*, 2009.

[38] P. W. Kervin, D. Hall, M. Bolden and J. Toth, "Phase Angle: What is it Good for?," in *AMOS Technical Conference*, 2010.

[39] A. N. Cox, Ed., Allen's Astrophysical Quantities, Fourth ed., New York: Springer-Verlag, 2000.

[40] M. R. Spiegel and J. Liu, Mathematical Handbook of Formulas and Tables, Second ed., McGraw-Hill, 1999.

[41] R. E. Walpole, R. H. Myers, S. L. Myers and K. Ye, Probability & Statistics for Engineers & Scientists, Eighth ed., Upper Saddle River: Pearson Prentice Hall, 2007.